

KUANG Yu-ping

QCD Multipole Expansion and Hadronic Transitions in Heavy Quarkonium Systems

© Higher Education Press and Springer-Verlag 2006

Abstract We review the developments of the multipole expansion approach in quantum chromodynamics and its applications to hadronic transitions and some radiative decays of heavy quarkonia. Theoretical predictions are compared with updated experimental results.

Keywords multipole expansion, quantum chromodynamics, heavy quarkonia, hadronic

PACS numbers 12.38.Lg, 13.25.Gv, 13.30.Eg

1 Introduction

Heavy quarkonia are the simplest objects used for studying the physics of hadrons because of their nonrelativistic nature. Although the spectra of heavy quarkonium systems $c\bar{c}$ and $b\bar{b}$ have been successfully explained by certain quantum chromodynamics (QCD) motivated potential models, some of their decays concerning nonperturbative QCD are difficult to deal with. Hadronic transitions

$$\Phi_I \rightarrow \Phi_F + h \quad (1)$$

are of this kind. In Eq. (1), Φ_I , Φ_F and h stand for the initial state quarkonium, the final state quarkonium, and the emitted light hadron(s), respectively. Hadronic transitions are important decay modes of heavy quarkonia. For instance, the branching ratio for $\psi' \rightarrow J/\psi + \pi + \pi$ is approximately 50%.

In the $c\bar{c}$ and $b\bar{b}$ systems, the typical mass difference $M_{\Phi_I} - M_{\Phi_F}$ is around a few hundred MeVs, so that the typical momentum of the light hadron(s) h is low. So far as the coupled-channel effect is not concerned, the light hadron(s) h are converted from the gluons emitted by the heavy quark Q or antiquark \bar{Q} in the transition. Thus, the typical momentum of the emitted gluons is also low, and

thus perturbative QCD does not work in these processes. Certain nonperturbative approaches are thus needed for studying hadronic transitions. In this article, we review the theoretical framework and applications of a feasible approach, QCD multipole expansion (QCDME), which works quite well in predicting hadronic transition rates in the $c\bar{c}$ and $b\bar{b}$ systems. In addition to hadronic transitions, QCDME can also lead to successful results in certain radiative decay processes such as $J/\psi \rightarrow \gamma\eta$ and $J/\psi \rightarrow \gamma\eta'$.

This paper is organized as follows. In Section 2, we review the theoretical framework and the formulation of QCDME. Section 3 deals with applications of QCDME to various hadronic transition processes in the nonrelativistic single-channel approach including hadronic transitions between S -wave quarkonia, between P -wave quarkonia, $\pi\pi$ transition of the D -wave quarkonia, and the search for the spin-singlet P -wave quarkonium h_c through hadronic transition. Section 4 is on the nonrelativistic coupled-channel theory of hadronic transitions. In Section 5, we show how QCDME makes successful predictions for the radiative decays $J/\psi \rightarrow \gamma\eta$ and $J/\psi \rightarrow \gamma\eta'$, etc. A summary is given in Section 6.

2 QCD multipole expansion

Multipole expansion in electrodynamics has been widely used for studying radiation processes in which the electromagnetic field is radiated from local sources. If the radius a of a local source is smaller than the wavelength λ of the radiated electromagnetic field such that $a/\lambda \sim ak < 1$ (k stands for the momentum of the photon), ak can be a good expansion parameter, i.e., we can expand the electromagnetic field in powers of ak . This is the well-known multipole expansion. In classical electrodynamics, the coefficient of the $(ak)^l$ term in the multipole expansion contains a factor $1/[(2l+1)!!]$. Hence multipole expansion actually works better than expected by simply estimating the size of $(ak)^l$.

Due to the nonrelativistic nature of heavy quarkonia, the bound states of a heavy quark Q and its antiquark \bar{Q} can be calculated by solving the Schrödinger equation with a

KUANG Yu-ping (✉)
Center for High Energy Physics and Department of Physics,
Tsinghua University,
Beijing 100084, China
E-mail: ypkuang@mail.tsinghua.edu.cn

given potential model, and the bound states are labeled by the principal quantum number n , the orbital angular momentum L , the total angular momentum J , and the spin multiplicity σ ($\sigma = 1$ or 3), i.e., $n^\sigma L_J$. The typical radius $a = \sqrt{\langle r^2 \rangle}$ of the $c\bar{c}$ and $b\bar{b}$ quarkonia obtained in this way is of the order of 10^{-1} fm. With such a small radius, the idea of multipole radiation can be applied to the soft gluon emissions in hadronic transitions. Consider an emitted gluon with a momentum k . For typical hadronic transition processes, k is approximately a few hundred MeVs, so that ak is of the order of 10^{-1} . Thus, multipole expansion works for hadronic transition processes. Note that the convergence of QCDME does not depend on the value of the QCD coupling constant g_s . Therefore, QCDME is a feasible approach to the soft gluon emissions in hadronic transitions (1).

QCDME has been studied by many authors [1–6]. The gauge-invariant formulation is given in [5]. Let $\psi(x)$ and $A_\mu^a(x)$ be the quark and gluon fields, respectively. Following [5], we introduce

$$\begin{aligned}\Psi(\mathbf{x}, t) &= U^{-1}(\mathbf{x}, t)\psi(x) \\ \frac{\lambda_a A_\mu^a(\mathbf{x}, t)}{2} &= U^{-1}(\mathbf{x}, t)\frac{\lambda_a A_\mu^a(x)}{2}U(\mathbf{x}, t) \\ &\quad - \frac{i}{g_s}U^{-1}(\mathbf{x}, t)\partial_\mu U(\mathbf{x}, t)\end{aligned}\quad (2)$$

where $U(x, t)$ is defined by [6]

$$U(\mathbf{x}, t) \equiv P \exp \left[i g_s \int_X^x \frac{\lambda_a}{2} A^a(x', t) \cdot d\mathbf{x}' \right] \quad (3)$$

in which P is the path-ordering operation, the line integral is along the straight-line segment connecting the two ends, $X \equiv (x_1 + x_2)/2$ is the center of mass position of Q and \bar{Q} , and x denotes x_1 or x_2 . With these transformed fields, the part of the QCD Lagrangian related to the heavy quarks becomes [5]

$$\begin{aligned}\mathcal{L}_Q &= \int \bar{\Psi} \left[\gamma^\mu \left(i\partial_\mu - g_s \frac{\lambda_a}{2} A_\mu^a \right) - m \right] \Psi d^3x - \frac{1}{2} \frac{g_s^2}{4\pi} \\ &\quad \int \sum_{a=0}^8 \bar{\Psi}(\mathbf{x}_1, t) \gamma^0 \frac{\lambda_a}{2} \Psi(\mathbf{x}_1, t) \\ &\quad \left| \frac{1}{\mathbf{x}_1 - \mathbf{x}_2} \right| \bar{\Psi}(\mathbf{x}_2, t) \gamma^0 \frac{\lambda_a}{2} \Psi(\mathbf{x}_2, t) d^3x_1 d^3x_2\end{aligned}\quad (4)$$

where $\lambda_0/2 \equiv 1$. Note that the transformed quark field $\Psi(\mathbf{x}, t)$ is dressed with gluons through $U^{-1}(\mathbf{x}, t)$ defined in Eq. (3). We see from Eq. (4) that the dressed quark field $\Psi(\mathbf{x}, t)$ serves as the *constituent quark* field interacting via the static coulomb potential in the potential model. In addition, it is the transformed gluon field A_μ^a (not the original

A_μ^a) that appears in the covariant derivative in Eq. (4). A_μ^a contains non-Abelian contributions through $U(\mathbf{x}, t)$.

Following [5], we generalize the coulomb potential in Eq. (4) to the static potential including the confining potential in potential models, and we write down the following effective Lagrangian [5]

$$\begin{aligned}\mathcal{L}_Q^{\text{eff}} &= \int \bar{\Psi} \left[\gamma^\mu \left(i\partial_\mu - g_s \frac{\lambda_a}{2} A_\mu^a \right) - m \right] \Psi d^3x - \frac{1}{2} \\ &\quad \int \sum_{a=0}^8 \bar{\Psi}(\mathbf{x}_1, t) \gamma^0 \frac{\lambda_a}{2} \Psi(\mathbf{x}_1, t) \\ &\quad \left[\delta_{a0} V_1(|\mathbf{x}_1 - \mathbf{x}_2|) + (1 - \delta_{a0}) \right. \\ &\quad \left. V_2(|\mathbf{x}_1 - \mathbf{x}_2|) \right] \bar{\Psi}(\mathbf{x}_2, t) \gamma^0 \frac{\lambda_a}{2} \Psi(\mathbf{x}_2, t) d^3x_1 d^3x_2\end{aligned}\quad (5)$$

where $V_1(|\mathbf{x}_1 - \mathbf{x}_2|)$ is the static potential (including the confining potential) between Q and \bar{Q} in the color singlet state, and $V_2(|\mathbf{x}_1 - \mathbf{x}_2|)$ is the static potential between Q and \bar{Q} in the color octet state. This $\mathcal{L}_Q^{\text{eff}}$ relates the QCD Lagrangian to the potential models.

Now we consider the *multipole expansion*. Inside the quarkonium, $|x - X| \leq a$. Thus we can make an expansion by expanding the gluon field $A_\mu^a(x, t)$ in the Taylor series of $x - X$ at the center of mass position X . The Taylor series is an expansion in powers of the operators $(x - X) \cdot \nabla$ and $(x - X) \times \nabla$ applying to the gluon field. After operating on the gluon field with the gluon momentum k , these operators are of the order of ak . This is QCDME. It has been shown in [5] that this operation leads to

$$A_0^a(\mathbf{x}, t) = A_0^a(\mathbf{X}, t) - (\mathbf{x} - \mathbf{X}) \cdot \mathbf{E}^a(\mathbf{X}, t) + \dots \quad (6)$$

$$A_i^a(\mathbf{x}, t) = -\frac{1}{2}(\mathbf{x} - \mathbf{X}) \times \mathbf{B}^a(\mathbf{X}, t) + \dots \quad (7)$$

where \mathbf{E}^a and \mathbf{B}^a are color electric and color magnetic fields, respectively.

In [5], the corresponding Hamiltonian was derived based on the above formulation. This is more convenient in using the nonrelativistic perturbation theory. The obtained Hamiltonian is [5]

$$H_{QCD}^{\text{eff}} = H_{QCD}^{(0)} + H_{QCD}^{(1)} \quad (8)$$

where

$$H_{QCD}^{(0)} = \int \Psi^\dagger(\mathbf{x}_1, t) \Psi(\mathbf{x}_1, t) \hat{H} \Psi^\dagger(\mathbf{x}_2, t) \Psi(\mathbf{x}_2, t) d^3x_1 d^3x_2 \quad (9)$$

with

$$\begin{aligned} \hat{H} \equiv & -\frac{1}{2m_Q}(\partial_1^2 + \partial_2^2 + V_1(|\mathbf{x}_1 - \mathbf{x}_2|) \\ & + \sum_{a=1}^8 \frac{\lambda_a}{2} \frac{\bar{\lambda}_a}{2} V_2(|\mathbf{x}_1 - \mathbf{x}_2|) + 2m_Q \end{aligned} \quad (10)$$

and

$$\begin{aligned} H_{\text{QCD}}^{(1)} = & H_1 + H_2 \\ H_1 \equiv & Q_a A_0^a(\mathbf{X}, t) \\ H_2 \equiv & -d_a \cdot \mathbf{E}^a(\mathbf{X}, t) - m_a \cdot \mathbf{B}^a(\mathbf{X}, t) + \dots \end{aligned} \quad (11)$$

in which

$$Q_a \equiv g_E \int \Psi^\dagger(\mathbf{x}, t) \frac{\lambda_a}{2} \Psi(\mathbf{x}, t) d^3x \quad (12)$$

$$\mathbf{d}_a \equiv g_E \int (\mathbf{x} - \mathbf{X}) \Psi^\dagger(\mathbf{x}, t) \frac{\lambda_a}{2} \Psi(\mathbf{x}, t) d^3x \quad (13)$$

$$\mathbf{m}_a \equiv \frac{g_M}{2} \int (\mathbf{x} - \mathbf{X}) \times \Psi^\dagger(\mathbf{x}, t) Y \frac{\lambda_a}{2} \Psi(\mathbf{x}, t) d^3x \quad (14)$$

are the color charge, color electric dipole moment, and color magnetic dipole moment of the $Q\bar{Q}$ system, respectively. Note that Eq. (5) is regarded as an effective Lagrangian. Considering that the heavy quark may have an anomalous magnetic moment, we have taken in Eqs. (12), (13), and (14) the symbols g_E and g_M to denote the effective coupling constants for the electric and magnetic

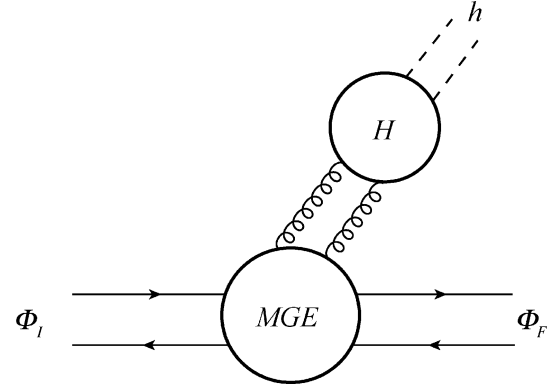


Fig. 1 A typical hadronic transition in the single-channel approach

multipole gluon emissions, respectively. We shall see later in Section 3 that taking α_E and α_M as two parameters is needed phenomenologically.

We are going to take $H_{\text{QCD}}^{(0)}$ as the zeroth-order Hamiltonian and take $H_{\text{QCD}}^{(1)}$ as a perturbation. This is different from the ordinary perturbation theory since $H_{\text{QCD}}^{(0)}$ is not a free field Hamiltonian. $H_{\text{QCD}}^{(0)}$ contains strong interactions in the potentials in \hat{H} , so that the eigenstates of $H_{\text{QCD}}^{(0)}$ are bound states rather than free field states. For a given potential model, the zeroth-order solution can be obtained by solving the Schrödinger equation with the given potential. Moreover, we see from Eqs. (12), (13), and (14) that only H_2 in $H_{\text{QCD}}^{(1)}$ is of $O(ak)$, while H_1 is of $O((ak)^0)$. Thus, we should keep all orders of H_1 in the perturbation expansion.

The general formula for the S matrix element between the initial state $|I\rangle$ and the final state $|F\rangle$ in this expansion has been given in [6], which is

$$\langle F|S|I\rangle = -i2\pi\delta(E_F + \omega_F - E_I) \left\langle F \left| H_2 \frac{1}{E_I - H_{\text{QCD}}^{(0)} + i\partial_0 - H_1} H_2 \cdots H_2 \frac{1}{E_I - H_{\text{QCD}}^{(0)} + i\partial_0 - H_1} H_2 \right| I \right\rangle \quad (15)$$

where ω_F is the energy of the emitted gluons. This is the basis of the study of hadronic transitions in QCDME. Explicit evaluation of the S matrix elements in various cases will be presented in Section 3.

3 Predictions for hadronic transitions in the single-channel approach

In this section, we shall show the predictions for hadronic transition rates in the single-channel approach (inclusion of coupled-channel contributions will be given in

Section 4). In this approach, the amplitude of hadronic transitions (1) is diagrammatically shown in Fig. 1 in which there are two complicated vertices, namely, the vertex of multipole gluon emissions (MGE) from the heavy quarks and the vertex of hadronization (H) describing the conversion of the emitted gluons into light hadron(s). The MGE vertex is at the scale of the heavy quarkonium, and it depends on the property of the heavy quarkonium. The H vertex is at the scale of the light hadron(s) and is independent of the property of the heavy quarkonium. In the following, we shall treat them separately.

3.1 Hadronic transitions between S -wave quarkonia

Let us first consider the case of $\pi\pi$ transitions between S -wave quarkonia, $n_I^3S_1 \rightarrow n_F^3S_1 + \pi + \pi$. These processes are dominated by double electric-dipole transitions (E1E1). The transition amplitude can be obtained from the S matrix element (15). With certain algebra, we obtain [5–7]

$$\mathcal{M}_{E1E1} = i \frac{g_E^2}{6} \left\langle \Phi_F h \left| \bar{\mathbf{x}} \cdot \mathbf{E} \frac{1}{E_I - H_{\text{QCD}}^{(0)} - iD_0} \bar{\mathbf{x}} \cdot \mathbf{E} \right| \Phi_I \right\rangle \quad (16)$$

where $\bar{\mathbf{x}}$ is the separation between Q and \bar{Q} , and $(D_0)_{bc} \equiv \delta_{bc} \partial_0 - g_s f_{abc} A_0^a$. Let us insert a complete set of intermediate states with the principal quantum number K and the orbital angular momentum L . Then Eq. (16) can be written as

$$\mathcal{M}_{E1E1} = i \frac{g_E^2}{6} \sum_{KLK'L'} \left\langle \Phi_F h \left| \bar{\mathbf{x}} \cdot \mathbf{E} \right| KL \right\rangle \left\langle KL \left| \frac{1}{E_I - H_{\text{QCD}}^{(0)} - iD_0} \right| K'L' \right\rangle \left\langle K'L' \left| \bar{\mathbf{x}} \cdot \mathbf{E} \right| \Phi_I \right\rangle \quad (17)$$

According to the angular momentum selection rule, the intermediate states must have $L = L' = 1$. The intermediate states in the hadronic transition are the states after the emission of the first gluon and before the emission of the second gluon shown in Fig. 1, i.e. they are states with a gluon and a color octet $Q\bar{Q}$. There is strong interaction between the gluon and the color octet $Q\bar{Q}$ since they all carry colors. Thus, these states are the so-called hybrid states. It is difficult to calculate these hybrid states from the first principles of QCD, so we shall take a reasonable model for it. The model should (a) reasonably reflect the main properties of the hybrid states and (b) contain as few unknown parameters as possible in order not to affect the predictive power of the theory. There is a quark confining string (QCS) model [8] satisfying these requirements. The QCS model is a one-dimensional string model in which the strong confining force between Q and \bar{Q} is described by the ground-state string, and gluon excitation effects are described by the vibrations of the string [8]. Our intermediate states $Q\bar{Q}g$ are thus described by the first vibrational mode in this model. The QCS model is not the only one satisfying the above requirements. Another possible model satisfying the requirements is the MIT bag model for the hybrid states. Hadronic transitions with the MIT bag model as the model for the intermediate states has been studied in [9]. It is shown that with the same input data, the predictions in this model are very close to those in the QCS

model, although the absolute, intermediate-state energy eigenvalues in the bag model are much higher than those in the QCS model. Thus, the predictions are not sensitive to the specific energy spectrum of the intermediate states. In the following, we take the calculations with the QCS model as examples. Explicit calculations of the first vibrational mode as the intermediate states are given in [7]. With this model, the transition amplitude (17) becomes [7]

$$\mathcal{M}_{E1E1} = i \frac{g_E^2}{6} \sum_{KL} \frac{\langle \Phi_F | \bar{\mathbf{x}}_K | KL \rangle \langle KL | \bar{\mathbf{x}}_L | \Phi_I \rangle}{E_I - E_{KL}} \langle \pi\pi | E_K^a E_L^a | 0 \rangle \quad (18)$$

where E_{KL} is the energy eigenvalue of the intermediate vibrational state $|KL\rangle$. We see that, in this approach, the transition amplitude contains two factors: namely, the heavy quark MGE factor (the summation) and the H factor $\langle \pi\pi | E_K^a E_L^a | 0 \rangle$. The first factor concerns the wave functions and energy eigenvalues of the initial- and final-state quarkonia and the intermediate states. These can be calculated for a given potential model. Let us now consider the treatment of the second factor. The scale of the H factor is the scale of light hadrons, which is very low. Therefore, the calculation of this matrix element is highly nonperturbative. So far, there is no reliable way of calculating this H factor from the first principles of QCD. Therefore, we take a phenomenological approach based on an analysis of the structure of this matrix element using PCAC and soft pion technique in [10]. In the center-of-mass frame, the two pion momenta q_1 and q_2 are the only independent variables describing this matrix element. According to [10], we can write this matrix element as [7]

$$\begin{aligned} & \frac{g_E^2}{6} \langle \pi_\alpha(q_1) \pi_\beta(q_2) | E_K^a E_L^a | 0 \rangle \\ &= \frac{\delta_{\alpha\beta}}{\sqrt{(2\omega_1)(2\omega_2)}} \left[C_1 \delta_{kl} q_1^\mu q_{2\mu} + C_2 \right. \\ & \quad \left. \left(q_{1k} q_{2l} + q_{1l} q_{2k} - \frac{2}{3} \delta_{kl} \mathbf{q}_1 \cdot \mathbf{q}_2 \right) \right] \end{aligned} \quad (19)$$

where C_1 and C_2 are two unknown constants. In the rest frame of Φ_I (the center-of-mass frame), for a given $\pi\pi$ invariant mass $M_{\pi\pi}$, the C_1 term is isotropic (S -wave), while the C_2 term is angular dependent (D -wave). In the nonrelativistic single-channel approach, the MGE factor in Eq. (18) is proportional to δ_{kl} due to orbital angular momentum conservation so that only the C_1 term contributes to the S -state to S -state transitions. In this case, the $n_I^3S_1 \rightarrow n_F^3S_1 + \pi + \pi$ transition rate can be expressed as [7]

$$\Gamma(n_I^3S_1 \rightarrow n_F^3S_1 \pi\pi) = |C_1|^2 G |f_{n_I n_F 0}^{111}|^2 \quad (20)$$

where the phase-space factor G is [7]

$$G \equiv \frac{3}{4} \frac{M_{\Phi_F}}{M_{\Phi_I}} \pi^3 \int K \sqrt{1 - \frac{4m_\pi^2}{M_{\pi\pi}^2} (M_{\pi\pi}^2 - 2m_\pi^2)^2} dM_{\pi\pi}^2 \quad (21)$$

with

$$K \equiv \frac{\sqrt{(M_{\Phi_I} + M_{\Phi_F})^2 - M_{\pi\pi}^2} \sqrt{(M_{\Phi_I} - M_{\Phi_F})^2 - M_{\pi\pi}^2}}{2M_{\Phi_I}} \quad (22)$$

and

$$f_{n_I l_I n_F l_F}^{LP_I P_F} \equiv \sum_K \frac{\int R_F(r) r^{P_F} R_{KL}^*(r) r^2 dr \int R_{KL}^*(r') r^{P_I} R_I(r') r'^2 dr'}{M_I - E_{KL}} \quad (23)$$

in which R_I , R_F and R_{KL} are radial wave functions of the initial, final, and intermediate vibrational states, respectively. These radial wave functions are calculated from the Schrödinger equation with a given potential model.

Now there is only one overall unknown constant C_1 left in this transition amplitude, and it can be determined by taking a well-measured hadronic transition rate as an input. So far, the best measured S -state to S -state $\pi\pi$ transition rate is $\Gamma(\psi' \rightarrow J/\psi \pi\pi)$. The updated experimental value is [11]

$$\begin{aligned} \Gamma_{\text{tot}}(\psi') &= 281 \pm 17 \text{ keV} \\ B(\psi' \rightarrow J/\psi \pi^+ \pi^-) &= (31.8 \pm 1.1)\% \\ B(\psi' \rightarrow J/\psi \pi^0 \pi^0) &= (18.8 \pm 1.2)\% \end{aligned} \quad (24)$$

We take this as an input to determine C_1 . Then we can predict all the S -state to S -state $\pi\pi$ transitions rates in the Υ system. Since the transition rate (20) depends on the potential model through the amplitude (23), the determined value of $|C_1|$ is model dependent. In the following, we take the Cornell Coulomb plus linear potential model [12] and the Buchmüller–Grunberg–Tye (BGT) potential model [13] as examples to show the determined $|C_1|$ and the predicted rates of $\Upsilon' \rightarrow \Upsilon\pi\pi$, $\Upsilon'' \rightarrow \Upsilon\pi\pi$, and $\Upsilon'' \rightarrow \Upsilon'\pi\pi$. The results are listed in Table 1.¹ We see that the predicted ratios $\Gamma(\Upsilon'' \rightarrow \Upsilon\pi\pi)/\Gamma(\Upsilon' \rightarrow \Upsilon\pi\pi) \approx 1.2/7.8 = 0.15$ and $\Gamma(\Upsilon'' \rightarrow \Upsilon'\pi\pi)/\Gamma(\Upsilon' \rightarrow \Upsilon\pi\pi) \approx 0.53/7.8 = 0.07$ in the BGT model are close to the corresponding experimental values $\Gamma(\Upsilon'' \rightarrow \Upsilon\pi\pi)/\Gamma(\Upsilon' \rightarrow \Upsilon\pi\pi) \approx 1.72/12.0 = 0.14$ and $\Gamma(\Upsilon'' \rightarrow \Upsilon'\pi\pi)/\Gamma(\Upsilon' \rightarrow \Upsilon\pi\pi) \approx 1.26/12.0 = 0.11$.

¹The calculated results are given in Ref. [7]. However, the updated results listed in Table 1 are larger than those in Ref. [7] by approximately a factor of 1.3 because the updated experimental value of $\Gamma(\psi' \rightarrow J/\psi \pi\pi)$ is larger than the old experimental value used in Ref. [7] by approximately a factor of 1.3.

Table 1 The determined $|C_1|^2$ and the predicted rates $\Gamma(\Upsilon' \rightarrow \Upsilon\pi\pi)$, $\Gamma(\Upsilon'' \rightarrow \Upsilon\pi\pi)$, and $\Gamma(\Upsilon'' \rightarrow \Upsilon'\pi\pi)$ (in keV) in the Cornell model and the BGT model. The corresponding updated experimental values of the transition rates quoted from [11] are also listed for comparison.

	Cornell	BGT	Experimental
$ C_1 ^2$	83.4×10^{-6}	67.8×10^{-6}	
$\Gamma(\Upsilon' \rightarrow \Upsilon\pi\pi)$ /keV	8.6	7.8	12.0 ± 1.8
$\Gamma(\Upsilon'' \rightarrow \Upsilon\pi\pi)$ /keV	0.44	1.2	1.72 ± 0.35
$\Gamma(\Upsilon'' \rightarrow \Upsilon'\pi\pi)$ /keV	0.78	0.53	1.26 ± 0.40

However, the predicted absolute partial widths are smaller than the corresponding experimental values by roughly a factor of (50-70)%. Moreover, when the $M_{\pi\pi}$ distributions are considered, the situation will be more complicated. We shall deal with these issues in Section 4.

Note that the phase space factor G in $\Upsilon'' \rightarrow \Upsilon\pi\pi$ is much larger than that in $\Upsilon' \rightarrow \Upsilon\pi\pi$, $G(\Upsilon'' \rightarrow \Upsilon\pi\pi)/G(\Upsilon' \rightarrow \Upsilon\pi\pi) = 33$. So one may naively expect that $\Gamma(\Upsilon'' \rightarrow \Upsilon\pi\pi) > \Gamma(\Upsilon' \rightarrow \Upsilon\pi\pi)$. However, we see from the experimental values in Table 1 that $\Gamma(\Upsilon'' \rightarrow \Upsilon\pi\pi)/\Gamma(\Upsilon' \rightarrow \Upsilon\pi\pi) \approx 1.72/12.2 = 0.14$. The reason why our predictions for this ratio is close to the experimental value is that the contributions from various intermediate states to the overlapping integrals in the summation in f_{3010}^{111} [cf. Eq. (23)] *drastically cancel* each other because the Υ'' wave function contains two nodes. This is a *characteristic* of this type of intermediate-state models (QCS or bag model). To see this, let us take a simplified model for the intermediate states and look at its prediction. If we make a simplification assumption that the variation of the factor $1/(E_I - H_{\text{QCD}}^{(0)} - iD_0)$ in Eq. (17) is sufficiently slow such that it can be approximately represented by a constant that can be taken out of the summation, the summations \sum_{KL} and $\sum_{K'L'}$ in Eq. (17) can then be carried out and the double overlapping integrals in the numerator in Eq. (23) reduces to a single integration $\int R_{\Upsilon''}^*(r) r^2 R_{\Upsilon'}(r) r^2 dr$. This simplified model predicts a rate $\Gamma(\Upsilon'' \rightarrow \Upsilon\pi\pi)$ larger than the experimental value by orders of magnitude [7]. Therefore, taking a reasonable model for the intermediate states is crucial for obtaining successful predictions in the QCDME approach to the MGE factor.

The transitions $n_I^3 S_1 \rightarrow n_F^3 S_1 + \eta$ are contributed by $E1M2$ and $M1M1$ transitions and are dominated by the $E1M2$ transition. The transition amplitude is

$$\begin{aligned} \mathcal{M}_{E1M2} &= -\frac{i}{2m_Q} \frac{g_{\text{EGM}}}{6} \sum_{KL} \\ &\frac{\langle \Phi_F | \bar{x}_k | KL \rangle \langle KL | S_i \bar{x}_m | \Phi_I \rangle + \langle \Phi_F | S_i \bar{x}_m | KL \rangle \langle KL | \bar{x}_k | \Phi_I \rangle}{E_I - E_{KL}} \\ &\langle \eta | E_k^a \partial_m B_l^a | 0 \rangle \end{aligned} \quad (25)$$

where S is the total spin of the quarkonium. The MGE matrix element is proportional to δ_{km} . Similar to the idea in Eq. (19), we can phenomenologically parameterize the hadronization factor according to its Lorentz structure as [14]

$$\frac{g_{\text{EGM}}}{6} \langle \eta(q) | E_k^a \partial_k B_l^a | 0 \rangle = i(2\pi)^{3/2} C_3 q_l \quad (26)$$

in which the phenomenological constant can be determined by taking the data [11]

$$\begin{aligned} \Gamma_{\text{tot}}(\psi') &= 277 \pm 22 \text{ keV} \\ B(\psi' \rightarrow J/\psi \eta) &= (3.17 \pm 0.21)\% \end{aligned} \quad (27)$$

as input, and so we can predict the rates for $\Upsilon' \rightarrow \Upsilon \eta$ and $\Upsilon'' \rightarrow \Upsilon \eta$. This is equivalent to

$$\Gamma(\Upsilon(n_I^3 S_1) \rightarrow \Upsilon \eta) = \frac{\left| \frac{f_{n_I 010}^{111}(b\bar{b})}{m_b} \right|^2}{\left| \frac{f_{2010}^{111}(c\bar{c})}{m_c} \right|^2} \frac{|q(b\bar{b})|^3}{|q(c\bar{c})|^3} \Gamma(\psi' \rightarrow J/\psi \eta) \quad (28)$$

where $q(b\bar{b})$ and $q(c\bar{c})$ are the momenta of η in $\Upsilon(n_I^3 S_1) \rightarrow \Upsilon \eta$ and $\psi' \rightarrow J/\psi \eta$, respectively. Taking the BGT model as an example to calculate the ratio of transition amplitudes in Eq. (28), we obtained

$$\begin{aligned} \Gamma(\Upsilon' \rightarrow \Upsilon \eta) &= 0.022 \text{ keV} \\ \Gamma(\Upsilon'' \rightarrow \Upsilon \eta) &= 0.011 \text{ keV} \end{aligned} \quad (29)$$

These are consistent with the present experimental bounds [11]

$$\begin{aligned} \Gamma(\Upsilon' \rightarrow \Upsilon \eta) &< 0.086 \text{ keV} \\ \Gamma(\Upsilon'' \rightarrow \Upsilon \eta) &< 0.058 \text{ keV} \end{aligned} \quad (30)$$

We can also compare the ratios $R' \equiv \Gamma(\Upsilon' \rightarrow \Upsilon \eta) / \Gamma(\psi' \rightarrow J/\psi \eta)$ and $R'' \equiv \Gamma(\Upsilon'' \rightarrow \Upsilon \eta) / \Gamma(\psi' \rightarrow J/\psi \eta)$ with the recent experimental measurements. Recently, Collaboration at the Beijing Spectrometer (BES) at Beijing Electron-Positron Collider has obtained an accurate measurement of $\Gamma(\psi' \rightarrow J/\psi \eta)$ and $\Gamma(\psi' \rightarrow J/\psi \pi^0)$ [15]. With the new BES data and the bounds on $\Gamma(\Upsilon' \rightarrow \Upsilon \eta)$ and $\Gamma(\Upsilon'' \rightarrow \Upsilon \eta)$ [11], the experimental bounds on R' and R'' are [15]

$$R' |_{\text{expt}} < 0.009 \quad R'' |_{\text{expt}} < 0.006 \quad (31)$$

Taking the BGT model to calculate the ratios R' and R'' , we obtain

$$R' |_{\text{BGT}} = 0.002 \quad R'' |_{\text{BGT}} = 0.001 \quad (32)$$

These are consistent with the new experimental bounds (31).

3.2 $\pi\pi$ Transitions between P -wave quarkonia

Let us consider the hadronic transitions $2^3P_{J_I} \rightarrow 1^3P_{J_F} + \pi + \pi$. For simplicity, we use the symbol $\Gamma(J_I \rightarrow J_F)$ to denote $\Gamma(2^3P_{J_I} \rightarrow 1^3P_{J_F} \pi\pi)$. These are also dominated by E1E1 transitions. The obtained results are [5,7]

$$\begin{aligned} \Gamma(0 \rightarrow 0) &= \frac{1}{9} |C_1|^2 G \left| f_{2111}^{011} + 2f_{2111}^{211} \right|^2 \\ \Gamma(0 \rightarrow 1) &= \Gamma(1 \rightarrow 0) = 0 \\ \Gamma(0 \rightarrow 2) &= 5\Gamma(2 \rightarrow 0) = \frac{10}{27} |C_2|^2 H \left| f_{2111}^{011} + \frac{1}{5} f_{2111}^{211} \right|^2 \\ \Gamma(1 \rightarrow 1) &= \Gamma(0 \rightarrow 0) + \frac{1}{4} \Gamma(0 \rightarrow 2) \\ \Gamma(1 \rightarrow 2) &= \frac{5}{3} \Gamma(2 \rightarrow 1) = \frac{3}{4} \Gamma(0 \rightarrow 2) \\ \Gamma(2 \rightarrow 2) &= \Gamma(0 \rightarrow 0) + \frac{7}{20} \Gamma(0 \rightarrow 2) \end{aligned} \quad (33)$$

where the phase-space factor H is

$$\begin{aligned} H &= \frac{1}{20} \frac{M_{\Phi_F}}{M_{\Phi_I}} \pi^3 \int K \sqrt{1 - \frac{4m_\pi^2}{M_{\pi\pi}}} \left[(M_{\pi\pi}^2 - 4m_\pi^2)^2 \right. \\ &\quad \left. \left(1 + \frac{2}{3} \frac{K^2}{M_{\pi\pi}^2} \right) + \frac{8K^4}{15M_{\pi\pi}^4} (M_{\pi\pi}^4 + 2m_\pi^2 M_{\pi\pi}^2 + 6m_\pi^4) \right] \\ &\quad dM_{\pi\pi}^2, \end{aligned} \quad (34)$$

with K defined in Eq. (22).

Now the rates in Eq. (33) depend on both C_1 and C_2 . We know that C_1 has been determined by the input (24). So far, there is no well-measured hadronic transition rate available for determining the ratio C_2/C_1 . At present, to make predictions, we can only take certain approximations to estimate C_2/C_1 theoretically. The approximation taken in [7] is to assume that the H factor $\langle \pi\pi | E_k^a E_l^a | 0 \rangle$ can be approximately expressed as

$$\langle \pi\pi | E_k^a E_l^a | 0 \rangle \propto \langle gg | E_k^a E_l^a | 0 \rangle \quad (35)$$

i.e., $\langle \pi\pi | E_k^a E_l^a | 0 \rangle$ approximately contains a factor $\langle gg | E_k^a E_l^a | 0 \rangle$ and another factor describing the conversion of the two gluons into $\pi\pi$, which is assumed to be approximately independent of the pion momenta in the hadronic transitions under consideration. The right-hand side of

Eq. (35) can be easily calculated. Comparing the obtained result with the form (19), we obtain

$$C_2/C_1 \approx 3 \quad (36)$$

in such an approximation. This is a crude approximation that can only be regarded as an order of magnitude estimate, so it is likely that $C_2/C_1 \sim O(1)$ rather than $O(10^{-1})$ or $O(10)$. A reasonable range of C_2/C_1 is

$$1 \lesssim C_2/C_1 \lesssim 3 \quad (37)$$

With this range of C_2/C_1 , the obtained transition rates $\Gamma(J_I \rightarrow J_F)$ of $\chi_b(2^3P_{J_I}) \rightarrow \chi_b(1^3P_{J_F})\pi\pi$ in the Cornell model [12] and the BGT model [13] are listed in Table 2. The relations between different $\Gamma(J_I \rightarrow J_F)$ given in Eq. (33) reflect the symmetry in the E1E1 multipole expansion [5], so that experimental tests of these relations are of special interest. Very recently, Collaboration at the detector CLEO at Cornell Electron-Positron Storage Ring reported a preliminary observation of the hadronic transitions $\chi_b(2^3P_{J_I}) \rightarrow \chi_b(1^3P_{J_F})\pi\pi$ for $J_I = J_F = 1$ and 2 [16]. However, the values of the rates have not been reported yet.

3.3 $\pi\pi$ Transitions of D -wave quarkonia

$\psi(3770)$ (or ψ'') is commonly regarded as essentially the $1D$ state of charmonium. It lies above the $D\bar{D}$ threshold, so that it is usually believed that $\psi(3770)$ mainly decays into the open-channel $D\bar{D}$. Experimental observations show that the directly measured $\psi(3770)$ production cross section at e^+e^- colliders is [17,18]

$$\sigma(\psi(3770)) = 7.5 \pm 0.8 \text{ nb} \quad (38)$$

while the $e^+e^- \rightarrow \psi(3770) \rightarrow D\bar{D}$ cross section is [19]

$$\sigma(\psi(3770) \rightarrow D\bar{D}) = 5.0 \pm 0.5 \text{ nb}. \quad (39)$$

This discrepancy may indicate that there are considerable non- $D\bar{D}$ decay modes of $\psi(3770)$. One of the possible non- $D\bar{D}$ decay modes is the hadronic transition $\psi(3770) \rightarrow J/\psi\pi\pi$. Theoretical studies of hadronic transitions of the D -wave quarkonia have been carried out by several authors in different approaches leading to quite different predictions [7,20–23]. In the following, we briefly

Table 2 Predicted transition rates $\Gamma(J_I \rightarrow J_F)$ of $\chi_b(2^3P_{J_I}) \rightarrow \chi_b(1^3P_{J_F})\pi\pi$ with the parameter range (37) in the Cornell [12] and the BGT models [13]

Model	$\Gamma(J_I \rightarrow J_F) / \text{keV}$				
	$\Gamma(0 \rightarrow 0)$	$\Gamma(0 \rightarrow 2)$	$\Gamma(1 \rightarrow 1)$	$\Gamma(1 \rightarrow 2)$	$\Gamma(2 \rightarrow 2)$
Cornell	0.4	0.004–0.04	0.4	0.003–0.03	0.4
BGT	0.4	0.002–0.02	0.4	0.001–0.01	0.4

review the approach given in [22,23], and compare the predictions with the recent experimental result and with other approaches.

The measured leptonic width of $\psi(3770)$ is (0.26 ± 0.04) keV [11]. If we simply regard $\psi(3770)$ as a pure $1D$ state of charmonium, the predicted leptonic width will be smaller than the experimental value by an order of magnitude. Therefore people consider $\psi(3770)$ as a mixture of charmonium states [22–24]. State mixing is an important consequence of the coupled-channel theory, especially for states close to or beyond the open-channel threshold. Take a successful coupled-channel model, the unitary quark model (UQM) [25], as an example. In this model, $\psi(3770)$ is a mixture of many S -wave and D -wave states of charmonium, but the main ingredients are the $\psi(1D)$ and $\psi(2S)$ states. Neglecting the small ingredients, we can write ψ' and $\psi(3770)$ as

$$\begin{aligned} \psi' &= \psi(2S) \cos \theta + \psi(1D) \sin \theta \\ \psi(3770) &= -\psi(2S) \sin \theta + \psi(1D) \cos \theta \end{aligned} \quad (40)$$

The UQM gives $\theta \approx -8^\circ$ [25]. Instead of taking a specific coupled-channel model, we take a phenomenological approach determining the mixing angle θ by fitting the ratio of the leptonic width of ψ' and $\psi(3770)$. The leptonic widths of $\psi(2S)$ and $\psi(1D)$ are proportional to the wave function at the origin $\psi_{2S}(0)$ and the second derivative of the wave function at the origin $(5/\sqrt{2})[(d^2\psi_{1D}(0)/dr^2)/2m_c^2]$, respectively. Therefore the determination of θ depends on the potential model. Here we take two potential models as illustration, namely, the Cornell potential model [12] and the improved QCD motivated potential model by Chen and Kuang (CK) [26], which leads to more successful phenomenological results. The determined values of θ are

$$\begin{aligned} \text{Cornell} : \theta &= -10^\circ \\ \text{CK} : \theta &= -12^\circ \end{aligned} \quad (41)$$

These are all consistent with the UQM value. There can also be an alternative solution with $\theta \sim 30^\circ$, but it is ruled out by the measured $M_{\pi\pi}$ distribution of $\psi' \rightarrow J/\psi + \pi + \pi$.

This transition is also dominated by E1E1 gluon emission. The transition rate is [22]

$$\begin{aligned} \Gamma(\psi(3770) \rightarrow J/\psi\pi\pi) &= |C_1|^2 \left[\sin^2 \theta G(\psi') |f_{2010}^{111}(\psi')|^2 + \frac{4}{15} \left| \frac{C_2}{C_1} \right|^2 \right. \\ &\quad \left. \cos^2 \theta H(\psi'') |f_{1210}^{111}(\psi'')|^2 \right] \end{aligned} \quad (42)$$

This transition rate depends on the potential model through the amplitudes f_{2010}^{111} , f_{1210}^{111} and the value of C_2/C_1 . We take the Cornell model [12] and the CK model [26] as examples. Taking the possible range for C_2/C_1 given in Eq. (37), we obtain the values of $\Gamma(\psi(3770) \rightarrow J/\psi + \pi^+ +$

Table 3 The predicted transition rate $\Gamma(\psi(3770) \rightarrow J/\psi + \pi^+ + \pi^-)$ (in keV) in the Cornell and CK models with the updated input data [Eq. (24)]

Model	$\Gamma(\psi(3770) \rightarrow J/\psi\pi^+\pi^-)$ /keV
Cornell	26–139
CK	32–147

π^-) listed in Table 3.² Note that $S-D$ mixing only affects a few percent of the rate, so that the rate is essentially $\Gamma(\psi(1D) \rightarrow J/\psi\pi^+\pi^-)$.

Recently, BES has measured the rate $\Gamma[\psi(3770) \rightarrow J/\psi + \pi^+ + \pi^-]$ based on 27.7 pb^{-1} data of $\psi(3770)$. The measured branching ratio is [27]

$$B(\psi(3770) \rightarrow J/\psi + \pi^+ + \pi^-) = (0.34 \pm 0.14 \pm 0.09)\% \quad (43)$$

With the total width [11]

$$\Gamma_{\text{tot}}(\psi(3770)) = 23.6 \pm 2.7 \text{ MeV} \quad (44)$$

the partial width is [27]

$$\Gamma_{\text{BES}}(\psi(3770) \rightarrow J/\psi + \pi^+ + \pi^-) = 80 \pm 32 \pm 21 \text{ keV} \quad (45)$$

This is in agreement with the theoretical predictions in Table 3. Taking the BES data [Eq. (45)] and Eq. (42) to determine C_2/C_1 , we obtain

$$C_2/C_1 = 2_{-1.3}^{+0.7} \quad (46)$$

This shows that C_2/C_1 is really of $O(1)$.

Very recently, CLEO-c also detected the channel $\psi(3770) \rightarrow J/\psi + \pi^+ + \pi^-$ with higher precision, and the measured branching ratio is [28]

$$B(\psi(3770) \rightarrow J/\psi + \pi^+ + \pi^-) = (0.214 \pm 0.025 \pm 0.022)\% \quad (47)$$

With the $\psi(3770)$ total width (44), the partial width is

$$\Gamma(\psi(3770) \rightarrow J/\psi + \pi^+ + \pi^-) = 50.5 \pm 16.9 \text{ keV} \quad (48)$$

We can also determine C_2/C_1 from Eqs. (48) and (42), and the result is

$$C_2/C_1 = 1.52_{-0.45}^{+0.35} \quad (49)$$

²The values listed in Table 3 are larger than those given in [22,23] since the updated input data is larger.

This is consistent with the value (46) determined from the BES data, but with higher precision.

An alternative way of calculating this kind of transition rate taking the approach to the H factor proposed by the papers in [4] was carried out in [21]. The so obtained transition rate is smaller than the above theoretical prediction by two orders of magnitude. Thus, it strongly disagrees with Eqs. (45) and (48). Therefore the approach given in [4] is ruled out by the BES and CLEO-c experiments.

For the Υ system, state mixings are much smaller [25]. Neglecting state mixings, the $\Upsilon(1D) \rightarrow \Upsilon(1S) + \pi^+ + \pi^-$ transition rate is proportional to $[C_2/C_1]^2$. Taking the determined values of C_2/C_1 in Eqs. (46) and (49), we obtain the corresponding transition rates: $1.3 \text{ keV} \leq \Gamma(\Upsilon(1D) \rightarrow \Upsilon(1S) + \pi^+ + \pi^-) \leq 14 \text{ keV}$ [from Eq. (46)] and $2.0 \text{ keV} \leq \Gamma(\Upsilon(1D) \rightarrow \Upsilon(1S) + \pi^+ + \pi^-) \leq 5.0 \text{ keV}$ [from Eq. (49)]. The lower values in these ranges are consistent with the CLEO bound [29]. Improved measurement of the $\Upsilon(1D) \rightarrow \Upsilon(1S) + \pi^+ + \pi^-$ rate is desired.

3.4 Searching for the h_c States

The spin-singlet P -wave states (1^1P_1) are of special interest since the difference between the mass of the 1^1P_1 state and the center of gravity of the 1^3P_J states $M_{\text{c.o.g}} = (5M_{1^3P_2} + 3M_{1^3P_1} + M_{1^3P_0})/9$ gives useful information about the spin-dependent interactions between the heavy quark and antiquark. There have been various experiments searching for the h_c ($\psi(1^1P_1)$) state.

In the $\bar{p}p$ collision, h_c can be directly produced. In 1992, the E760 Collaboration claimed seeing a significant enhancement in $\bar{p}p \rightarrow J/\psi + \pi^0$ at $\sqrt{s} = 3526.2 \text{ MeV}$, which was supposed to be a candidate of h_c [30]. However, such an enhancement has not been confirmed by the successive E835 experiment from a careful scan in this region with significantly higher statistics [31]. Instead, the E835 experiment recently found the h_c state via another channel $\bar{p}p \rightarrow h_c \rightarrow \eta_c \gamma$, and the measured resonance mass is $M_{h_c} = 3525.8 \pm 0.2 \pm 0.2 \text{ MeV}$ with a width $\Gamma_{h_c} \lesssim 1 \text{ MeV}$ [31]. The measured production rate is consistent with the theoretical range given in [14] (see [31]).

At the e^+e^- colliders, the h_c state cannot be produced directly in the s -channel due to its CP quantum number. Because of the limited phase space, the best way of searching for the h_c state at CLEO-c or BES is through the isospin violating hadronic transition [14,23,32]

$$\psi' \rightarrow h_c + \pi^0 \quad (50)$$

Theoretical calculations of this transition rate considering $S-D$ mixing in ψ' and suggestions for tagging the h_c are given in [23]. Here we give a brief review of it.

The process $\psi' \rightarrow h_c + \pi^0$ is dominated by E1M1 transition. The transition amplitude is

$$\mathcal{M}_{\text{E1M1}} = i \frac{g_{\text{E}g\text{M}}}{6} \frac{1}{2m_c} \sum_{KL} \frac{\langle h_c | \bar{x}_k | KL \rangle \langle KL | (s_c - s_{\bar{c}})_l | \psi' \rangle + \langle h_c | (s_c - s_{\bar{c}})_l | KL \rangle \langle KL | \bar{x}_k | \psi' \rangle}{M_{\psi'} - E_{KL}} \langle \pi^0 | E_k B_l | 0 \rangle \quad (51)$$

where s_c and $s_{\bar{c}}$ are spins of c and \bar{c} , respectively. The phenomenological approach to the H factor used above does not work in the present case since there is no accurate measurement of E1M1 transition rate available as input datum to determine the phenomenological parameter so far. Fortunately, evaluation of this special H factor from QCD turns out to be easy. Since π^0 is a pseudoscalar, the H factor $\langle \pi^0 | E_k B_l | 0 \rangle$ is nonvanishing only when $E_k B_l = \delta_{kl} \mathbf{E} \cdot \mathbf{B} / 3$, and $\mathbf{E} \cdot \mathbf{B}$ is related to the axial-vector anomaly. Therefore

$$\begin{aligned} \langle \pi^0(\eta) | \alpha_s E_k B_l | 0 \rangle &= \frac{1}{3} \delta_{kl} \langle \pi^0(\eta) | \alpha_s \mathbf{E} \cdot \mathbf{B}^a | 0 \rangle \\ &= \frac{1}{12} \delta_{kl} \langle \pi^0(\eta) | \alpha_s F_{\mu\nu}^a \tilde{F}^{a\mu\nu} | 0 \rangle \end{aligned} \quad (52)$$

and the last matrix element can be evaluated by using the Gross–Treiman–Wilczek formula [33], which leads to

$$\begin{aligned} \langle \pi^0 | \alpha_s F_{\mu\nu}^a \tilde{F}^{a\mu\nu} | 0 \rangle &= \frac{4\pi}{\sqrt{2}} \frac{m_d - m_u}{m_d + m_u} f_\pi m_\pi^2 \\ \langle \eta | \alpha_s F_{\mu\nu}^a \tilde{F}^{a\mu\nu} | 0 \rangle &= \frac{4\pi}{\sqrt{6}} f_\pi m_\eta^2 \end{aligned} \quad (53)$$

in which the factor $(m_d - m_u)/(m_d + m_u)$ reflects the violation of isospin. To predict the transition rate with these expressions, we should determine the relations between the effective coupling constants $\alpha_E = g_E^2/4\pi$, $\alpha_M = g_M^2/4\pi$ and the coupling constant α_s appearing in Eqs. (52) and (53). With certain approximations, we can calculate the transition rates $\Gamma(\psi' \rightarrow J/\psi\pi\pi)$ and $\Gamma(\psi' \rightarrow J/\psi\eta)$ expressed in terms of α_E and α_M [7,14], so that α_E and α_M can be determined by taking the input data [Eqs. (24) and (27)].³ The determined α_E is approximately

$$\alpha_E \approx 0.6 \quad (54)$$

while the determination of α_M is quite uncertain because the approximation used in calculating $\Gamma(\psi' \rightarrow J/\psi\eta)$ is rather crude [14]. So we take a possible range [14]

$$\alpha_E \leq \alpha_M \leq 3\alpha_E \quad (55)$$

to estimate the rate. Since the value of α_E in Eq. (54) is just about the commonly estimated value of the strong coupling constant α_s at the light hadron scale, we simply take $\alpha_s \approx \alpha_E$. In this spirit, taking account of the S - D mixing (40) in ψ' , the transition rate of Eq. (50) is

$$\begin{aligned} \Gamma(\psi' \rightarrow h_c \pi^0) &= \frac{\pi^3}{143m_c^2} \left(\frac{\alpha_M}{\alpha_E} \right) \left| \cos \theta \left(f_{2011}^{110} + f_{2011}^{001} \right) \right. \\ &\quad \left. - \sqrt{2} \sin \theta \left(f_{1211}^{110} + f_{1211}^{201} \right) \right|^2 \frac{E_{h_c}}{M_{\psi'}} \\ &\quad \left[\frac{m_d - m_u}{m_d + m_u} f_\pi m_\pi^2 \right]^2 |\mathbf{q}_\pi| \end{aligned} \quad (56)$$

Here we have neglected the state mixing effect in h_c , which is small [25] since h_c is not close to the $D\bar{D}$ threshold. The numerical result in the CK potential model is [23]

$$\begin{aligned} \Gamma(\psi' \rightarrow h_c \pi^0) &= 0.06 \left(\frac{\alpha_M}{\alpha_E} \right) \text{ keV} \\ B(\psi' \rightarrow h_c \pi^0) &= (2.2 \pm 0.2) \left(\frac{\alpha_M}{\alpha_E} \right) \times 10^{-4} \end{aligned} \quad (57)$$

The calculation shows that the dependence of the transition rate on the potential model is mild.

We know that π^0 decays 99% into two photons. Thus the signal in Eq. (50) is $\psi' \rightarrow h_c \gamma\gamma$ with $M_{\gamma\gamma} = m_{\pi^0}$. If the momenta of the two photons can be measured with sufficient accuracy, one can look for the monotonic $M_{\gamma\gamma}$ as the signal. From the branching ratio in Eq. (57), we see that taking into account a 10% detection efficiency, we can observe hundreds of signal events for an accumulation of 10 millions of ψ' . The backgrounds are shown to be either small or can be clearly excluded [23]. Once the two photon energies ω_1 and ω_2 are measured, the h_c mass can be extracted from the relation $M_{h_c}^2 = M_{\psi'}^2 + m_{\pi^0}^2 - 2M_{\psi'}(\omega_1 + \omega_2)$.

³ In such an approach, it is not possible to simply take $\alpha_E = \alpha_M$ to fit the two input data. This is why we take α_E and α_M as two parameters in our whole approach. Furthermore, the updated input datum of $\Gamma(\psi' \rightarrow J/\psi\pi\pi)$ obtained from (24) is larger than the old value used in Ref. [7], so that the determined α_E in Eq. (54) is larger than the values listed in Ref. [7].

To have a clearer signal, one can further look at the decay product of h_c . It has been shown that the main decay channel of h_c is $h_c \rightarrow \eta_c \gamma$ [23], so that the easiest signal is $\psi' \rightarrow h_c \pi^0 \rightarrow \eta_c \gamma \gamma \gamma$. The branching ratio $B(h_c \rightarrow \eta_c \gamma)$ depends on the hadronic width of h_c . In [23], the hadronic width of h_c was studied both in the conventional perturbative QCD (PQCD) and in nonrelativistic QCD (NRQCD) approaches.

We first look at the PQCD result. With the hadronic width obtained from PQCD, Kuang [23] predicts

$$B(h_c \rightarrow \eta_c \gamma) = (88 \pm 2)\% \quad (58)$$

Combining Eqs. (57) and (58) with the possible range (55) of the undetermined parameter α_M/α_E , we obtain

$$\begin{aligned} \text{PQCD} : B(\psi' \rightarrow h_c \pi^0) \times B(h_c \rightarrow \eta_c \gamma) \\ = (1.9 - 5.8) \times 10^{-4} \end{aligned} \quad (59)$$

Signals considering the exclusive hadronic decay modes of η_c are also studied in [23].

Recently, CLEO-c has found the h_c state via the channel $\psi' \rightarrow h_c \pi^0 \rightarrow \eta_c \gamma \gamma \gamma$ [16,34]. The measured resonance mass is $M_{h_c} = 3524.4 \pm 0.6 \pm 0.4$ MeV [16,34], which is consistent with the E835 result at the 1σ level. The measured $B(\psi' \rightarrow h_c \pi^0) \times B(h_c \rightarrow \eta_c \gamma)$ is [16,34]

$$\begin{aligned} \text{CLEO-c} : B(\psi' \rightarrow h_c \pi^0) \times B(h_c \rightarrow \eta_c \gamma) \\ = (4.0 \pm 0.8 \pm 0.7) \times 10^{-4} \end{aligned} \quad (60)$$

which is in good agreement with the above theoretically predicted range (59). Future improved measurement with higher precision can serve as an input to determine the unknown parameter α_M/α_E .

NRQCD predicts a larger hadronic width of h_c , so it predicts a smaller branching ratio of $h_c \rightarrow \eta_c \gamma$. say $B(h_c \rightarrow \eta_c \gamma) = (41 \pm 3)\%$ [23], which leads to

$$\begin{aligned} \text{NRQCD} : B(\psi' \rightarrow h_c \pi^0) \times B(h_c \rightarrow \eta_c \gamma) \\ = (0.9 - 2.7) \times 10^{-4} \end{aligned} \quad (61)$$

This is also consistent with the CLEO-c result (60) to the present precision. We expect future CLEO-c experiments with higher precision to test the PQCD and NRQCD approaches. Since the H factor (53) in this $\psi' \rightarrow h_c \pi^0$ process is obtained from the Gross-Treiman-Wilczek relation without taking approximations, the agreement between Eqs. (59) and (60) implies that the above theoretical approach to the MGE factor in Eq. (51) is quite reasonable. CLEO-c has also studied some exclusive hadronic channels [16,34]. More accurate measurement of the branching ratios of these exclusive hadronic channels may also be compared with the corresponding predictions in [23] to test PQCD and NRQCD approaches.

4 Nonrelativistic coupled-channel approach to hadronic transitions

We know that an excited heavy quarkonium state lying above the open heavy flavor threshold can decay into a pair of heavy flavor mesons \mathcal{D} and $\bar{\mathcal{D}}$ (\mathcal{D} stands for the D mesons if the heavy quark is c , and stands for the B mesons if the heavy quark is b). This means that there must exist couplings between Φ , \mathcal{D} , and $\bar{\mathcal{D}}$ shown in Fig. 2. With such couplings taken into account, a complete theory of heavy quarkonia satisfying the requirement of *unitarity* should include not only the theory describing the discrete states Φ , but also the theory describing the continuous sector $\mathcal{D}\bar{\mathcal{D}}$ as well. Such a theory is the so-called coupled-channel theory.

It is hard to study the $\Phi - \mathcal{D} - \bar{\mathcal{D}}$ vertex shown in Fig. 2 from the first principles of QCD since it is an interaction vertex between three bound states. There are various models describing coupled-channel effects, and two well-accepted models are the Cornell coupled-channel model [12,35] and the UQM [25] mentioned in Section 3. The $\Phi - \mathcal{D} - \bar{\mathcal{D}}$ vertex in the UQM is taken to be the 3P_0 quark-pair-creation (QPC) mechanism [36], i.e., the creation of light quark pairs $q\bar{q}$ is supposed to have the vacuum quantum numbers $J^{PC} = 0^{++}$ (3P_0), and the vertex in Fig. 2 is described by the 3P_0 sector of the overlapping integral between the three bound-state wave functions with an almost universal coupling constant $\gamma_{\text{QPC}} \approx 3.03$ [36]. The parameters in the UQM are carefully adjusted so that the model gives good fit to the $c\bar{c}$ and $b\bar{b}$ spectra, leptonic widths, etc. It has been shown that the QPC model also gives not bad results for OZI-allowed productions of light mesons [36,37], which will be relevant in the calculation of the hadronic transition amplitudes in Fig. 3(e) and (f) in the coupled-channel theory. Thus, we take the UQM to discuss hadronic transitions in this section.

In the UQM, the whole Hilbert space is divided into two sectors, namely, the confined sector $|\Phi_0; \lambda\rangle$ labeled by the discrete quantum number λ (say σ, n, L, J) and the continuous sector $|\mathcal{D}\bar{\mathcal{D}}; \nu\rangle$ labeled by the continuous quantum number ν (say the momentum). The state $|\Phi_0; \lambda\rangle$ is

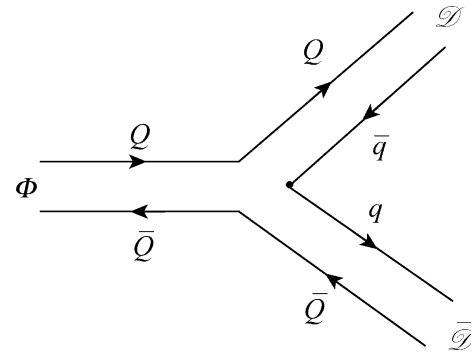


Fig. 2 Coupling of the heavy quarkonium Φ to its decay channel $\mathcal{D}\bar{\mathcal{D}}$

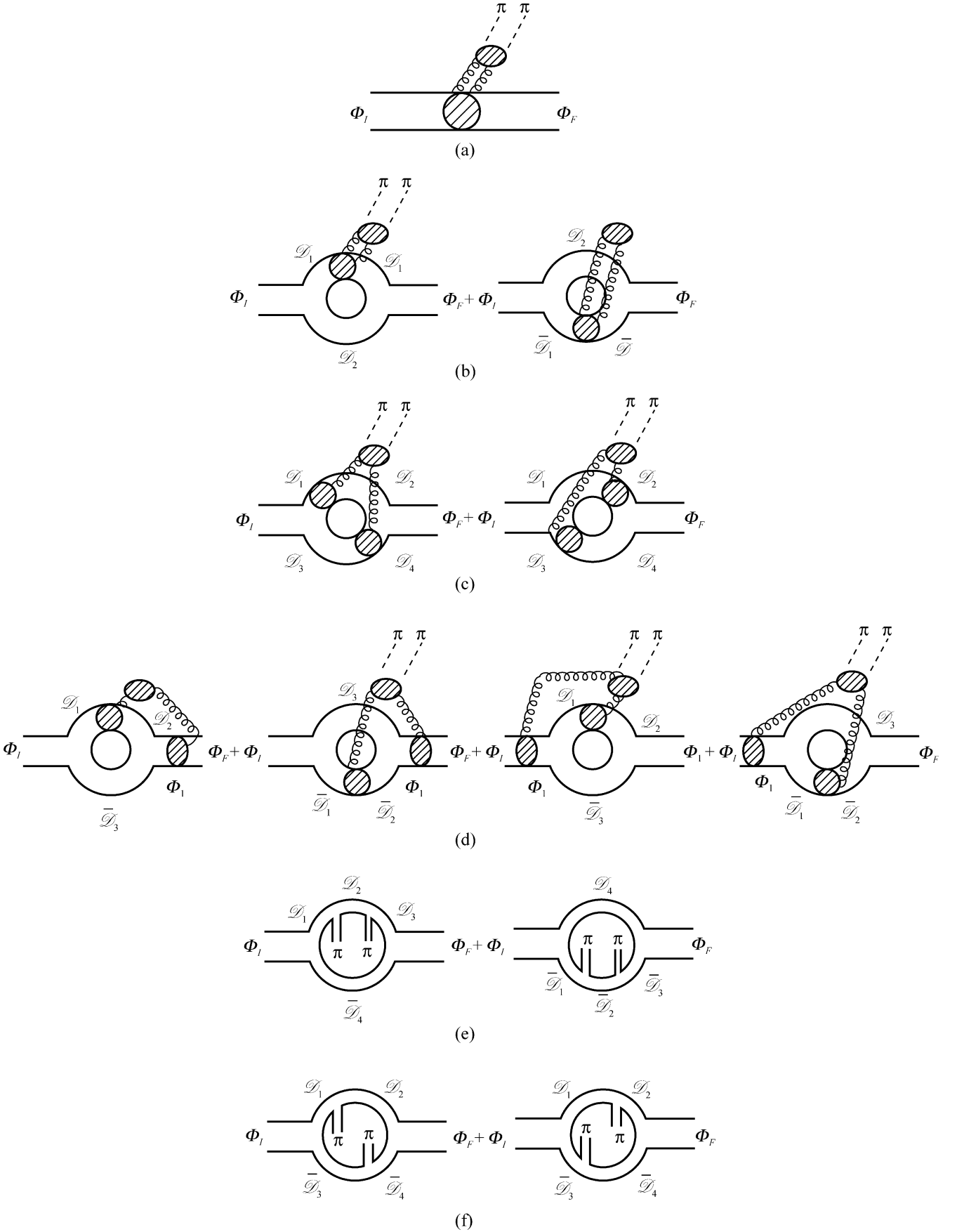


Fig. 3 Hadronic transitions in the coupled-channel approach. (e) and (f) are new transition mechanisms beyond the QCD multipole expansion. (From Zhou [38])

just the eigenstate of the Hamiltonian H_0 in the naive single-channel theory with the eigenvalue M_λ^0 (the bare mass); i.e.,

$$H_0|\Phi_0; \lambda\rangle = M_\lambda^0|\Phi_0; \lambda\rangle \quad (62)$$

and the state $|\mathcal{D}\bar{\mathcal{D}}; \nu\rangle$ is a state with two freely moving mesons \mathcal{D} and $\bar{\mathcal{D}}$, which is the eigenstate of the kinetic-energy Hamiltonian H_0^c with the energy eigenvalue E_ν ; i.e.,

$$H_0^c|\mathcal{D}\bar{\mathcal{D}}; \nu\rangle = E_\nu|\mathcal{D}\bar{\mathcal{D}}; \nu\rangle \quad (63)$$

The total Hamiltonian H of the system contains H_0 , H_0^c and the quark-pair-creation Hamiltonian H_{QPC} , which determines the OZI-allowed $\Phi - \mathcal{D} - \bar{\mathcal{D}}$ vertex and mixes the two sectors. H can be written as

$$H = \begin{pmatrix} H_0 & 0 \\ 0 & H_0^c \end{pmatrix} + \begin{pmatrix} 0 & H_{\text{QPC}}^\dagger \\ H_{\text{QPC}} & 0 \end{pmatrix} \quad (64)$$

where the first and second rows stand for the confined channel and the continuous channel, respectively. Note that

$$\begin{aligned} \langle \Phi_0; \lambda | H_{\text{QPC}} | \Phi_0; \lambda' \rangle &= 0 \\ \langle \mathcal{D}\bar{\mathcal{D}}; \nu | H_{\text{QPC}} | \mathcal{D}\bar{\mathcal{D}}; \nu' \rangle &= 0 \end{aligned} \quad (65)$$

With H_{QPC} introduced, there will be a self-energy $\Pi_{\lambda\lambda'}$ of the quarkonium Φ_0 contributed by virtual loops of \mathcal{D} mesons. This is shown in Fig. 4. The self-energy $\Pi_{\lambda\lambda'}$ is not necessarily diagonal, i.e., λ and λ' may be different. This causes the state mixings. For states below the threshold, the self-energy $\Pi_{\lambda\lambda'}$ is

$$\Pi_{\lambda\lambda'} = -\int \frac{\langle \Phi_0; \lambda | H_{\text{QPC}} | \mathcal{D}\bar{\mathcal{D}}; \nu \rangle \langle \mathcal{D}\bar{\mathcal{D}}; \nu | H_{\text{QPC}} | \Phi_0; \lambda' \rangle}{M_\lambda - E_\nu} d\nu. \quad (66)$$

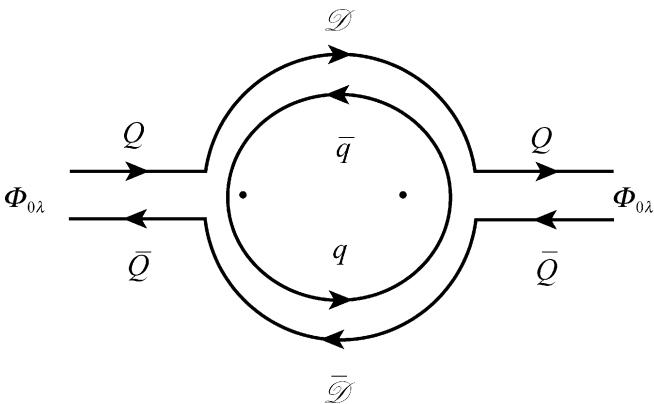


Fig. 4 The self-energy $\Pi_{\lambda\lambda'}$ from the \mathcal{D} meson loop

Now the total mass matrix of the quarkonium state is

$$M_{\lambda\lambda'} = M_\lambda^0 \delta_{\lambda\lambda'} + \Pi_{\lambda\lambda'} \quad (67)$$

Let $\alpha_{\lambda\lambda'}$ be the matrix diagonalizing $M_{\lambda\lambda'}$, and M_λ be the diagonal matrix element. The physical quarkonium state $|\Phi; \lambda\rangle$ is the eigenstate of H with the energy eigenvalue M_λ ; i.e.,

$$H|\Phi; \lambda\rangle = M_\lambda|\Phi; \lambda\rangle \quad (68)$$

The eigenstate $|\Phi; \lambda\rangle$ can be expressed as a superposition of $|\Phi_0; \lambda\rangle$ and $|\mathcal{D}\bar{\mathcal{D}}; \nu\rangle$:

$$|\Phi; \lambda\rangle = \sum_{\lambda'} \alpha_{\lambda\lambda'} |\Phi_0; \lambda'\rangle + \int c_\lambda(\nu) |\mathcal{D}\bar{\mathcal{D}}; \nu\rangle d\nu \quad (69)$$

in which all possible open heavy flavor mesons \mathcal{D} ($\bar{\mathcal{D}}$) composed of the heavy quark Q and all possible light quarks \bar{q} (q) should be included.

The state mixing coefficient $a_{\lambda\lambda'}$ is related to $\alpha_{\lambda\lambda'}$ by [25]

$$a_{\lambda\lambda'} = N_\lambda \alpha_{\lambda\lambda'}^T \quad (70)$$

where [25]

$$N_\lambda = \left[1 + \int \left| \frac{\langle \mathcal{D}\bar{\mathcal{D}}; \nu | H_{\text{QPC}} | \Phi_0; \lambda \rangle}{M_\lambda - E_\nu} \right|^2 d\nu \right]^{-1/2} \quad (71)$$

is a normalization coefficient, and N_λ^2 determines the probability of finding the confined sector $|\Phi_0; \lambda\rangle$ in the physical state $|\Phi; \lambda\rangle$. The calculation of α 's and N_λ 's is tedious, and the results for various $c\bar{c}$ and $b\bar{b}$ states are given in [25]. The mixing coefficient $c_\lambda(\nu)$ is related to $a_{\lambda\lambda'}$ by [25]

$$c_\lambda(\nu) = \sum_{\lambda'} a_{\lambda\lambda'} \langle \mathcal{D}\bar{\mathcal{D}}; \nu | H_{\text{QPC}} | \Phi_0; \lambda' \rangle / (M_\lambda - E_\nu) \quad (72)$$

In the single-channel approach, the energy eigenvalues M_λ^0 of high-lying quarkonium states predicted by potential models are usually higher than the experimental values. In the coupled-channel theory, the self-energy $\Pi_{\lambda\lambda'}$ usually causes $M_\lambda < M_\lambda^0$. Since coupled-channel corrections $M_\lambda - M_\lambda^0$ are unimportant for states lying much lower than the $\mathcal{D}\bar{\mathcal{D}}$ threshold but are relatively important for states close and above the $\mathcal{D}\bar{\mathcal{D}}$ threshold, coupled-channel theory does improve the prediction for the energy spectra. The UQM coupled-channel theory has been applied to obtain successful results of heavy quarkonium spectra, leptonic widths, etc. for the $c\bar{c}$ and $b\bar{b}$ systems [25].

The formulation of the theory of hadronic transitions in the framework of the UQM was given in [38]. Let $H_{\text{pair}} \equiv H_{\text{QPC}} + H_{\text{QPC}}^\dagger$, $\hat{H}_0 \equiv H_0$ for the confining sector and $\hat{H}_0 \equiv H_0^c$ for the continuous sector. In the framework of UQM, the S matrix element (15) becomes [38]

$$\langle F|S|I\rangle = -i2\pi\delta(E_F + \omega_F - E_I) \left\langle F \left| (H_2 + H_{\text{pair}}) \frac{1}{E_I - \hat{H}_0 + i\partial_0 - H_1} (H_2 + H_{\text{pair}}) \cdots (H_2 + H_{\text{pair}}) \frac{1}{E_I - \hat{H}_0 + i\partial_0 - H_1} (H_2 + H_{\text{pair}}) \right| I \right\rangle \quad (73)$$

For isospin-conserving $\pi\pi$ transitions (dominated by E1E1 gluon emissions), we take the electric dipole term in H_2 [Eq. (11)]. Note that, in Eq. (73), the creation of the two pions can come not only from the conversion of the two emitted gluons (OZI-forbidden mechanism) via the two H_2 's, but also from the OZI-allowed mechanism $\langle \mathcal{D}\bar{\mathcal{D}}\pi; \nu | H_{\text{QPC}} | \mathcal{D}\bar{\mathcal{D}}; \nu \rangle$ directly from the light quark lines [Fig. 3(e)–(f)]. Note that the two gluons can only convert into two pions (not one pion) due to isospin conservation. Thus these two pion creation mechanisms contribute separately. The $\pi\pi$ transition S matrix element between two physical quarkonium states $|\Phi; \lambda_I\rangle$ and $|\Phi; \lambda_F\rangle$ is [38]

$$\begin{aligned} & \langle \Phi; \lambda_F; \pi(\mathbf{k}_1)\pi(\mathbf{k}_2) | S | \Phi; \lambda_I \rangle \\ &= -i2\pi\delta(M_F + E_{\pi_1} + E_{\pi_2} - M_I) \\ & \sum_{\lambda'_i \lambda'_f} a_{\lambda_I \lambda'_i} a_{\lambda_F \lambda'_f} \left\langle \Phi_0; \lambda'_f; \pi(\mathbf{k}_1)\pi(\mathbf{k}_2) \right| \\ & \left[H_2 \frac{1}{M_I - \hat{H}_0 + i\partial_0 - H_1} H_2 \right. \\ & + H_{\text{QPC}}^\dagger \frac{1}{M_I - \hat{H}_0 + i\partial_0 - H_1} H_2 \\ & \frac{1}{M_I - \hat{H}_0 + i\partial_0 - H_1} H_2 \frac{1}{M_I - \hat{H}_0} H_{\text{QPC}} \\ & + H_2 \frac{1}{M_I - \hat{H}_0 + i\partial_0 - H_1} H_{\text{QPC}}^\dagger \frac{1}{M_I - \hat{H}_0 + i\partial_0 - H_1} H_2 \\ & \frac{1}{M_I - \hat{H}_0} H_{\text{QPC}} + H_{\text{QPC}}^\dagger \frac{1}{M_I - \hat{H}_0 + i\partial_0 - H_1} H_2 \\ & \frac{1}{M_I - \hat{H}_0 + i\partial_0 - H_1} H_{\text{QPC}} \frac{1}{M_I - \hat{H}_0 + i\partial_0 - H_1} \\ & H_2 + H_{\text{QPC}}^\dagger \frac{1}{M_I - \hat{H}_0} H_{\text{QPC}} \frac{1}{M_I - \hat{H}_0} \\ & \left. H_{\text{QPC}} \frac{1}{M_I - \hat{H}_0} H_{\text{QPC}} \right] \left| \Phi_0; \lambda'_i \right\rangle \end{aligned} \quad (74)$$

where E_{π_1} and E_{π_2} are energies of the two pions. The Feynman diagrams corresponding to the terms in Eq. (74) are shown in Fig. 3 in which Fig. 3(a)–(d) are diagrams corresponding to the first four terms in Eq. (74), and Fig. 3(e)–(f) are diagrams for the last term in Eq. (74). For convenience, we shall call the first four terms in Eq. (74) the MGE part, and call the last term in Eq. (74) the quark-pair-creation (QPC) part.

We see that Eq. (74) contains much more channels of $\pi\pi$ transitions than the single-channel theory does. In the MGE part, Fig. 3(a) is similar to Fig. 1 but with state mixings, so that the single-channel amplitude mentioned in Section 3.1 is only a part of the first term in Eq. (74). In the QPC part, the last term in Eq. (74) is a *new pion creation mechanism through H_{QPC} irrelevant to MGE*. Thus in the coupled-channel theory, $\pi\pi$ transitions between heavy quarkonium states are not merely described by QCME.

Since the state mixings and the QPC vertices depending on the bound-state wave functions are all different in the $c\bar{c}$ and the $b\bar{b}$ systems, the predictions for $\Gamma(\Upsilon' \rightarrow \Upsilon\pi\pi)$, $\Gamma(\Upsilon'' \rightarrow \Upsilon\pi\pi)$, and $\Gamma(\Upsilon'' \rightarrow \Upsilon'\pi\pi)$ by taking $\Gamma_{\text{exp}}(\psi' \rightarrow J/\psi\pi\pi)$ as input will be different from those in the single-channel theory. Such predictions were studied in [38] in which the same potential model as in [25] is taken for avoiding the tedious calculation of α 's and N_λ 's. Note that for a given QPC model, the QPC part in Eq. (74) is fixed, while the MGE part still contains an unknown parameter C_1 in its hadronization factor after taking the approximation (36). Since there is interference between the MGE part and the QPC part, the phase of C_1 will affect the result. Let

$$C_1 = |C_1| e^{i\vartheta} \quad (75)$$

Two input data are thus needed to determine $|C_1|$ and ϑ . In [38], the data of the transition rate and $M_{\pi\pi}$ distribution in $\psi' \rightarrow J/\psi\pi\pi$ are taken as the inputs. Considering the experimental errors in the $M_{\pi\pi}$ distribution, ϑ is restricted in the range $-1 \leq \cos \vartheta \leq -0.676$. The details of the calculation are given in [38] in which the \mathcal{D} meson states $D(B)$, $D^*(B^*)$, and $D^{**}(B^{**})$ are taken into account. The so predicted transition rates $\Gamma(\Upsilon' \rightarrow \Upsilon\pi\pi)$, $\Gamma(\Upsilon'' \rightarrow \Upsilon\pi\pi)$, and $\Gamma(\Upsilon'' \rightarrow \Upsilon'\pi\pi)$ for $\cos \vartheta = -1$ and $\cos \vartheta = -0.676$ are listed in Table 4 together with the updated experimental results for comparison.

Table 4 The predicted rates $\Gamma(\Upsilon' \rightarrow \Upsilon\pi\pi)$, $\Gamma(\Upsilon'' \rightarrow \Upsilon\pi\pi)$, and $\Gamma(\Upsilon'' \rightarrow \Upsilon'\pi\pi)$ (in keV) in the coupled-channel theory with $\cos \vartheta = -1$ and $\cos \vartheta = -0.676$. The corresponding updated experimental values of the transition rates quoted from [11] are also listed for comparison.

	Theoretical		Experimental
	$\cos \vartheta = -1$	$\cos \vartheta = -0.676$	
$\Gamma(\Upsilon' \rightarrow \Upsilon\pi\pi)$ (keV)	14	13	12.0 ± 1.8
$\Gamma(\Upsilon'' \rightarrow \Upsilon\pi\pi)$ (keV)	1.1	1.0	1.72 ± 0.35
$\Gamma(\Upsilon'' \rightarrow \Upsilon'\pi\pi)$ (keV)	0.1	0.3	1.26 ± 0.40

We see that the obtained $\Gamma(\Upsilon' \rightarrow \Upsilon\pi\pi)$ is in good agreement with the experiment, and the results of $\Gamma(\Upsilon'' \rightarrow \Upsilon\pi\pi)$ and $\Gamma(\Upsilon'' \rightarrow \Upsilon'\pi\pi)$ are in agreement with the experiments at the level of 2σ and 2.4σ , respectively.

Next we look at the predicted $M_{\pi\pi}$ distributions. It is pointed out in [39] that there is a tiny difference between the measured $M_{\pi\pi}$ distributions in $\psi' \rightarrow J/\psi \pi\pi$ and $\Upsilon' \rightarrow \Upsilon\pi\pi$. In the single-channel theory, the formulas for these $M_{\pi\pi}$ distributions are the same with the same value of $|C_1|$. Albrecht et al. [39] tried to explain the tiny difference by taking the approach to the H factor given in [4], in which there is a parameter κ that is supposed to run. However, the running of κ is not known theoretically, so that it is not clear whether the running of κ from the scale $M_{\psi'} - M_{J/\psi} = 590$ MeV to the scale $M_{\Upsilon'} - M_{\Upsilon} = 560$ MeV can really explain the tiny difference. Furthermore, as we have seen in Section 3.3, the approach given in [4] is ruled out by the recent BES and CLEO-c experiments. In the present coupled-channel theory, once the values of $|C_1|$ and ϑ are determined by the input data of $\psi' \rightarrow J/\psi \pi\pi$, the $M_{\pi\pi}$ distribution of $\Upsilon' \rightarrow \Upsilon\pi\pi$ is definitely predicted. The comparison of the predicted distribution with the experimental data given in [39] is shown in Fig. 5. We see that the agreement is good, so that the coupled-channel theory successfully predicts the tiny difference.

However, the situation of the $M_{\pi\pi}$ distributions of $\Upsilon'' \rightarrow \Upsilon\pi^+\pi^-$ and $\Upsilon'' \rightarrow \Upsilon'\pi^+\pi^-$ are more complicated. The single-channel theory predicts $M_{\pi\pi}$ distributions similar to Fig. 5 for these two processes, i.e., the distributions are peaked at the large $M_{\pi\pi}$ region. The CLEO data show a clear double-peaked shape for the $M_{\pi\pi}$ distribution of $\Upsilon'' \rightarrow \Upsilon\pi^+\pi^-$ [Fig. 6(a)] [40,41]. The coupled-channel theory does enhance the low- $M_{\pi\pi}$ region

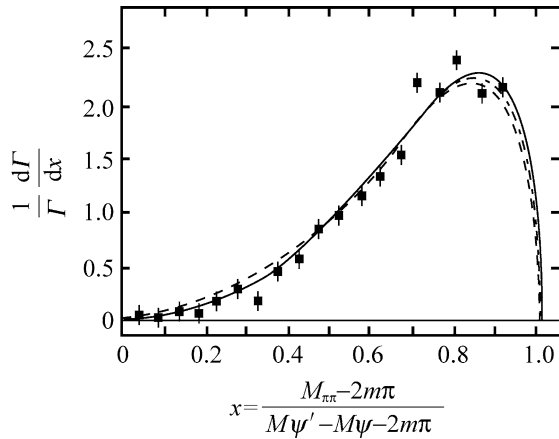


Fig. 5 Comparison of the coupled-channel theory predicted curve of $d\Gamma(\Upsilon' \rightarrow \{\Upsilon\pi\pi\})/dM_{\pi\pi}$ with the ARGUS data [39]. The solid and dashed-dotted lines stand for $\cos\theta = -1$ and $\cos\theta = -0.676$, respectively. The dashed line is the naive single-channel result for comparison. (From Zhou [38])

a little, but is far from giving a double-peaked shape, as is shown by the solid and dashed-dotted curves in Fig. 6(a). Actually, this situation is not only for the coupled-channel theory based on the UQM. The Cornell coupled-channel model is not substantially different from the UQM [38]. Compared with the UQM, the Cornell coupled-channel model leads to relatively larger S - S mixings but smaller S - D mixings after taking the same experimental inputs, so that the Cornell coupled-channel model gives even smaller enhancement in the low- $M_{\pi\pi}$ region. Thus, the transition $\Upsilon'' \rightarrow \Upsilon\pi^+\pi^-$ needs further investigation with new ideas, although the predicted transition rate $\Gamma(\Upsilon'' \rightarrow \Upsilon\pi^+\pi^-)$ is consistent with the CLEO data at the 2σ level.

There have been various attempts to explain the double-peaked shape. Voloshin [42] assumed the existence of a four-quark state Υ_1 having nearly the same mass as Υ'' and coupling strongly to $\Upsilon''\pi$ and $\Upsilon\pi$, and the dominant transition mechanism is suggested to be $\Upsilon'' \rightarrow \Upsilon_1 + \pi \rightarrow \Upsilon + \pi + \pi$, which enhances the low- $M_{\pi\pi}$ distribution. The branching ratio of $\Upsilon(4S) \rightarrow \Upsilon_1 + \pi$ is estimated to be roughly 1%, so that the assumption can be experimentally tested by searching for the Υ_1 state in $\Upsilon(4S)$ decays. This idea was carefully studied in [43], taking into account the final-state $\pi\pi$ interactions, and obtained a double-peaked shape, but the low- $M_{\pi\pi}$ peak was not at the desired position. A slightly modified model of this kind was proposed in [44]. So far, the assumed four-quark state is not found experimentally. Another attempt was made in [45], assuming that the coupled-channel contributions are strong enough in $\Upsilon'' \rightarrow \Upsilon\pi\pi$ that there is a considerably large QPC part in the transition amplitude, and the interference between it and the MGE part may form a double-peaked shape by adjusting the strength of the QPC part. However, as we mentioned above, the strength of the QPC part is fixed once a QPC model is given, and the systematic calculation in [38] shows that the QPC part is actually much smaller than what was expected in [45]. Recently, attempts were made to explain the double-peaked shape by certain models for a light σ meson resonance at around 500 MeV in the final-state $\pi\pi$ interactions with [46] and without [47] using the Breit-Wigner formula. By adjusting the free parameters in the models, the CLEO data on the $M_{\pi\pi}$ distributions in $\Upsilon'' \rightarrow \Upsilon\pi\pi$ and $\Upsilon'' \rightarrow \Upsilon'\pi\pi$ can be fitted. However, the models need to be tested in other processes. Therefore, the $\Upsilon'' \rightarrow \Upsilon\pi\pi$ transition is still an interesting process needing further investigation.

We would like to mention that the calculations mentioned above concern the wave functions of some excited states of heavy quarkonia, the heavy flavored mesons \mathcal{D} , and the pions. Nonrelativistic potential model calculations of these wave functions may not be so good. Therefore, the nonrelativistic coupled-channel theory of hadronic transitions in [38] still needs further improvement.

5 Application of QCD multipole expansion to radiative decays of J/ψ

In the preceding sections, QCD multipole expansion is applied to various hadronic transition processes in which the initial- and final-state quarkonia Φ_I and Φ_F are composed of the same heavy quarks. In this case, the dressed (constituent) quark field $\Psi(\mathbf{x}, t)$ does not actually need to be quantized. Now we generalize the QCDME theory to processes including heavy quark flavor changing and heavy quark pair annihilation or creation. Then the quantization of the $\Psi(\mathbf{x}, t)$ is needed. This has been studied in [6], and the canonical commutation relation obtained is [6]

$$[\Psi(\mathbf{x}, t), \Psi^\dagger(\mathbf{x}', t)] = \delta^3(\mathbf{x} - \mathbf{x}') \quad (76)$$

To include the electromagnetic and weak interactions, we generalize the Hamiltonian as

$$H = H_{\text{QCD}}^{(0)} + H_{\text{int}} \quad (77)$$

$$H_{\text{int}} = H_{\text{QCD}}^{(1)} + H_{\text{em}} + H_{\text{w}} \quad (78)$$

in which $H_{\text{QCD}}^{(0)}$ and $H_{\text{QCD}}^{(1)}$ are defined in Eqs. (9) and (11), and

$$\begin{aligned} H_{\text{em}} &= e \int d^3x \bar{\Psi}(\mathbf{x}, t) \gamma^\mu \mathcal{Q} A_\mu(\mathbf{x}, t) \Psi(\mathbf{x}, t) \\ H_{\text{w}} &= \int d^3x \left[\frac{g}{\sqrt{2}} \bar{\Psi}(\mathbf{x}, t) \gamma^\mu \frac{1-\gamma_5}{2} [t_+ W_\mu^+(x) + t_- W_\mu^-(x)] \Psi(\mathbf{x}, t) \right. \\ &\quad \left. + \frac{g}{\cos \theta_W} \bar{\Psi}(\mathbf{x}, t) \gamma^\mu \left(\frac{1-\gamma_5}{2} t_3 - \sin^2 \theta_W \mathcal{Q} \right) Z_\mu(x) \Psi(\mathbf{x}, t) \right] \end{aligned} \quad (79)$$

where \mathcal{Q} is the electric charge operator of the heavy quark, A_μ is the photon field, g and t_i are, respectively, the weak

$SU(2)$ coupling constant and generator, θ_W is the Weinberg angle, and $e = g \sin \theta_W$ is the electromagnetic coupling constant.

Let us take the application of the generalized theory to the radiative decay process $J/\psi \rightarrow \gamma + \eta$ as an example. This process has been studied in the framework of perturbative QCD and nonrelativistic quark model in [48], but the predicted rate is significantly smaller than the experimental value. We know that the momentum of the η meson in this process is $q_\eta = (M_{J/\psi}^2 - m_\eta^2)/(2M_{J/\psi}) = 1.5$ GeV. Suppose the η meson is converted from two emitted gluons from the heavy quark. The typical momentum of a gluon is then $k \sim q_\eta/2 \sim 750$ MeV. This is the momentum scale in which perturbative QCD does not work well but QCDME works [6]. Thus, we can calculate the rate of this decay process using QCDME. The Feynman diagrams for this process are shown in Fig. 7, in which the intermediate states marked between two vertical dotted lines are all treated as *bound states* in this approach. In this sense, this approach is nonperturbative, and for this reason the contributions of the three diagrams in Fig. 7 are different.

In QCDME, this process is dominated by the E1M2 gluon emissions. Thus, the H factor (conversion of the two gluons into η) is

$$g_{\text{EGM}} \langle \eta | E_j^a D_j B_i^a | 0 \rangle \quad (80)$$

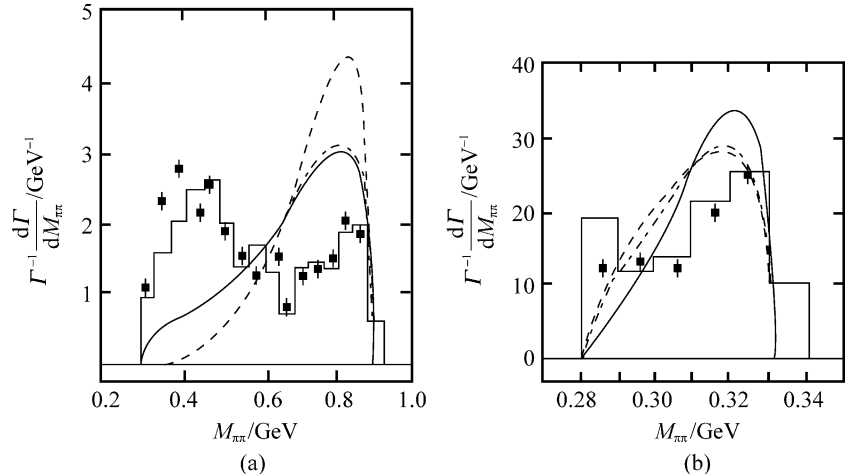
where $D_j \equiv \partial_j - g_s (\lambda_a/2) A_j^a$ is the covariant derivative. The operator in Eq. (80) can be written as

$$E_j^a D_j B_i^a = \partial_j (E_j^a B_i^a) - (D_j E_j^a) B_i^a$$

It is argued in [4] that the second term is smaller than the first term, so they suggested the approximation

$$g_{\text{EGM}} \langle \eta | E_j^a D_j B_i^a | 0 \rangle \approx i q_{\eta j} \langle \eta | E_j^a B_i^a | 0 \rangle \quad (81)$$

Fig. 6 Comparison of the coupled-channel theory predicted curves of $d\Gamma(\Upsilon'' \rightarrow \pi^+\pi^-)/dM_{\pi\pi}$ (a) and $d\Gamma(\Upsilon'' \rightarrow \Upsilon' \pi^+\pi^-)/dM_{\pi\pi}$ (b) with the CLEO data [40]. The solid and dashed-dotted lines stand for $\cos \theta = -1$ and $\cos \theta = -0.676$, respectively. The dashed line is the naive single-channel result for comparison. (From Zhou [38])



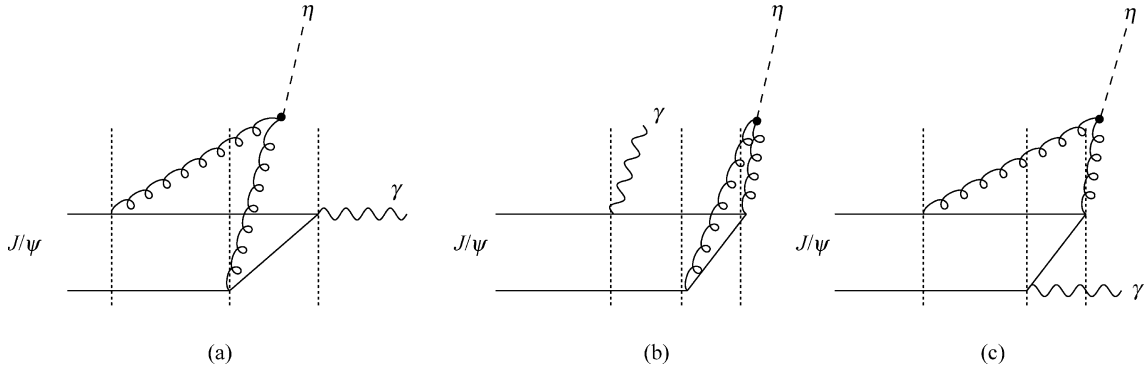


Fig. 7 Feynman diagrams for the radiative decay process $J/\psi \rightarrow \gamma + \eta$. The intermediate states between two vertical dotted lines are all bound states.

This matrix element can then be evaluated by using the Gross–Treiman–Wilczek formula [33], and we obtain [6]

$$g_{\text{EGM}} \langle \eta | E_j^a D_j B_i^a | 0 \rangle \approx i \frac{g_{\text{EGM}}}{g_s^2} \frac{4\pi^2}{3\sqrt{6}} q_\eta f_\pi m_\eta^2 (\cos \theta_P - \sqrt{2} \sin \theta_P) \delta_{ij} \quad (82)$$

where θ_P is the mixing angle in the pseudoscalar nonet; i.e.,

$$\eta = \eta_8 \cos \theta_P - \eta_1 \sin \theta_P, \quad \eta' = \eta_8 \sin \theta_P + \eta_1 \cos \theta_P, \quad (83)$$

with

$$\eta_8 = \frac{1}{\sqrt{6}} (\bar{u}\gamma_5 u + \bar{d}\gamma_5 d - 2\bar{s}\gamma_5 s) \quad (84)$$

$$\eta_1 = \frac{1}{\sqrt{3}} (\bar{u}\gamma_5 u + \bar{d}\gamma_5 d + \bar{s}\gamma_5 s)$$

As in Section 3.4, we take $\alpha_s \approx \alpha_E = 0.6$. It is shown in [6] that the contribution of Fig. 7(a) is larger than that of Fig. 7(b) and (c). Thus as an approximation, we only consider the main contribution of Fig. 7(a).

The calculated $J/\psi \rightarrow \gamma\eta$ rate is [6]

$$\Gamma(J/\psi \rightarrow \gamma\eta) = \frac{1}{6\pi} \left(\frac{\alpha_M}{\alpha_E} \right) \frac{|q_\eta|^3}{M_{J/\psi}} \left(\frac{2eQ}{3\sqrt{6}m_c} \right)^2 \left[\frac{4\pi^2}{3\sqrt{6}} f_\pi m_\eta^2 (\cos \theta_P - \sqrt{2} \sin \theta_P) \sum_n h_{10n0}^{111} \right]^2 \quad (85)$$

where

$$h_{n_l l_i n_l}^{LP_i P} \equiv \sum_K \frac{\langle R_{n_F} | r^P | R'_{KL} \rangle \langle R'_{KL} | r^{P_i} | R_{n_l i} \rangle}{(M_{J/\psi} - E_{n_l} - \omega_\eta)(M_{J/\psi} - E'_{KL})} f_{nl}(0) \quad (86)$$

in which $R_{n_l i}$, R_{nl} , and R'_{KL} are radial wave functions of the initial-, final-, and intermediate-quarkonium states in Fig. 7(a), respectively. $f_{nl}(0)$ is the wave function at the origin of the final-quarkonium state. We shall take into account the first five terms in the summation $\sum_n h_{10n0}^{111}$. As

it is well-known that $f_{n0}(0)$ can be determined by the datum of the related leptonic width $\Gamma(\psi(n^3S_1) \rightarrow e^+e^-)$. For $n = 1, 2$, the so determined $f_{10}(0)$ and $f_{20}(0)$ are smaller than the ones predicted by the Cornell potential model by almost the same factor 0.57 [12]. It is expected that this discrepancy may be explained by QCD corrections. For $n \geq 3$, the states are above the threshold and state mixings will be significant, so that the data of $\Gamma(\psi(n^3S_1) \rightarrow e^+e^-)$ are not useful. We expect that QCD corrections will not vary seriously with n , as is inspired by the cases of $n = 1, 2$. Then we can calculate $f_{10}(0), \dots, f_{50}(0)$ using the Cornell potential model and then multiply the obtained results by the same factor, 0.57, to obtain the correct values.

The factor $(\cos \theta_P - \sqrt{2} \sin \theta_P)$ in Eq. (82) concerns the effective η -g-g vertex in the hadronization $gg \rightarrow \eta$. This is somewhat similar to the effective η - γ - γ vertex in $\eta \rightarrow \gamma\gamma$. We may take the determined value of θ_P from the $\eta \rightarrow \gamma\gamma$ and $\eta' \rightarrow \gamma\gamma$ data, which is $\theta_P \approx -20^\circ$ [11]. With this value of θ_P , we get

$$\Gamma(J/\psi \rightarrow \gamma\eta) = 0.041 \left(\frac{\alpha_M}{\alpha_E} \right) \text{keV} \quad (87)$$

With the experimental datum $\Gamma_{\text{tot}}(J/\psi) = 91.0 \pm 3.2$ keV [11], we obtain

$$B(J/\psi \rightarrow \gamma\eta) = (4.5 \pm 0.2) \times 10^{-4} \left(\frac{\alpha_M}{\alpha_E} \right) \quad (88)$$

The experimental value of this branching ratio is [11]

$$B(J/\psi \rightarrow \gamma\eta) \Big|_{\text{expt}} = (8.6 \pm 0.8) \times 10^{-4}$$

We see that for $\alpha_M/\alpha_E \approx 1.9$, the predicted branching ratio agrees with the experimental value.

Note that the value of α_M/α_E and θ_P are not so certain, and we do not know how good the approximation (81) really is. To avoid these uncertainties, we can take the ratio of $\Gamma(J/\psi \rightarrow \gamma\eta)$ to another E1M2 transition rate $\Gamma(\psi' \rightarrow J/\psi\eta)$. The theoretical prediction is [6]

$$\begin{aligned} R_\eta &\equiv \frac{\Gamma(J/\psi \rightarrow \gamma\eta)}{\Gamma(\psi' \rightarrow J/\psi\eta)} \\ &= \frac{8}{81} (e\mathcal{Q})^2 |q_\eta(J/\psi \rightarrow \gamma\eta)|^3 / M_{J/\psi} \left| \sum_n h_{10n0}^{111} \right|^2 \\ &= \frac{2}{243} |q_\eta(\psi' \rightarrow J/\psi\eta)|^3 |f_{2010}^{111}|^2 \\ &= 0.012 \end{aligned} \quad (89)$$

In this ratio, the uncertainties mentioned above are all cancelled, so that R_η just tests the MGE mechanism in this approach. The corresponding experimental value is [11]

$$R_\eta \Big|_{\text{expt}} = 0.009 \pm 0.003 \quad (90)$$

We see that the agreement is at the 1σ level. Since we have seen in Section 3.4 that the calculation of the MGE factor mentioned in Section 3 is quite reasonable, the agreement of Eq. (89) with Eq. (90) implies that MGE mechanism for this radiative decay process is also reasonable.

The above approach can also be applied to the radiative decay process $J/\psi \rightarrow \gamma\eta'$. From Eq. (83) we see that the $J/\psi \rightarrow \gamma\eta'$ decay rate is

$$\begin{aligned} &\Gamma(J/\psi \rightarrow \gamma\eta') \\ &= \frac{1}{6\pi} \left(\frac{\alpha_M}{\alpha_E} \right) |q_{\eta'}|^3 \left(\frac{2e\mathcal{Q}}{3\sqrt{6}m_c} \right)^2 \left[\frac{4\pi^2}{3\sqrt{6}} f_\pi m_{\eta'}^2 \right. \\ &\quad \left. (\sqrt{2} \cos \theta_P + \sin \theta_P) \sum_n h_{10n0}^{111} \right]^2 \end{aligned} \quad (91)$$

Since there is no $\psi' \rightarrow J/\psi\eta'$ available (not enough phase space), we cannot have a ratio similar to R_η that exactly tests the MGE mechanism. We can define the ratio

$$\begin{aligned} R_{\eta'} &\equiv \frac{\Gamma(J/\psi \rightarrow \gamma\eta')}{\Gamma(\psi' \rightarrow J/\psi\eta)} \\ &= \left| \frac{q(J/\psi \rightarrow \gamma\eta')}{q(J/\psi \rightarrow \gamma\eta)} \right|^3 \\ &= \frac{m_\eta^2 (\sqrt{2} \cos \theta_P + \sin \theta_P)^2}{m_\eta^2 (\cos \theta_P - \sqrt{2} \sin \theta_P)^2} R_\eta. \end{aligned} \quad (92)$$

Taking $\theta_P \approx -20^\circ$ determined from the $\eta \rightarrow \gamma\gamma$ and $\eta' \rightarrow \gamma\gamma$ rates, we predict

$$R_{\eta'} = 0.044 \quad (93)$$

The corresponding experimental value of $R_{\eta'}$ is [11]

$$R_{\eta'} \Big|_{\text{expt}} = 0.044 \pm 0.010 \quad (94)$$

We see that this prediction is also in agreement with the experiment.

It has been shown in [6] that the contribution of the above mechanism to the isospin violating radiative decay $J/\psi \rightarrow \gamma + \pi^0$ is negligibly small. There is another important mechanism giving the main contribution to $J/\psi \rightarrow \gamma + \pi^0$. It is the ρ^0 meson dominance mechanism $J/\psi \rightarrow \rho^{0*} + \pi^0 \rightarrow \gamma + \pi^0$. This has been studied in [57], and the result is close to the experimental value.⁴

We would like to mention that this approach is not suitable for $\Upsilon \rightarrow \gamma\eta$ since the typical gluon momentum in this process is $k \sim q_\eta/2 \sim 2.4$ GeV, at which perturbative QCD works, while QCD multipole expansion does not. Studies of the processes $\Upsilon \rightarrow \gamma\eta$, $\Upsilon \rightarrow \gamma\eta'$ and $\Upsilon \rightarrow \gamma f_2(1270)$ have been carried out in [49]. Application of this approach to $\psi' \rightarrow \gamma\eta$ is more complicated since both relativistic and coupled-channel corrections are important in this process. Thus, development of a relativistic coupled-channel is desired.

QCDME can also be applied to study the direct photon spectrum in $J/\psi \rightarrow \gamma + \text{hadrons}$ near $x \simeq 1$, where $x \equiv 2\omega_\gamma/M$, with ω_γ the energy of the photon and M the mass of the quarkonium. Conventional study of the process $J/\psi(\Upsilon) \rightarrow \gamma + \text{hadrons}$ are based on perturbative QCD calculation of $J/\psi(\Upsilon) \rightarrow \gamma + g + g$ in the Born approximation [50]. The direct photon spectrum is expressed as

$$\frac{1}{\Gamma_{\text{tot}}} \frac{d\Gamma(J/\psi(\Upsilon) \rightarrow \gamma + \text{hadrons})}{dx}$$

For Υ , the obtained result is in good agreement with the experiment [51–53], while for J/ψ the obtained distribution is too hard, i.e., in the range $x > 0.8$, the obtained distribution is much larger than the experimental values [54]. In $J/\psi \rightarrow \gamma + \text{hadrons}$, the typical gluon momentum at $x \approx 1$ is $k \approx 770$ MeV, so that we can apply QCDME to it for $x \geq 0.9$. The calculation was done in [55], and the obtained direct photon spectrum for $x \geq 0.9$ is very close to the experimental values [55]. For $x < 0.9$, the typical gluon momentum is too large for QCDME to work. A successful theory for the whole range of x is still expected.

⁴ The contribution of the ρ^0 meson dominance mechanism to $J/\psi \rightarrow \gamma\eta$ is negligibly small because the branching ratio $B(J/\psi \rightarrow \rho^0 + \eta)$ is about two orders of magnitude smaller than $B(J/\psi \rightarrow \rho^0 + \pi^0)$.

Table 5 Summary of the predictions for transition and decay rates in the nonrelativistic QCD multipole expansion approach together with the corresponding experimental results for comparison

	Theoretical predictions	Experimental data	Places in the text
$\Gamma(\Upsilon' \rightarrow \Upsilon\pi\pi)$	13 keV	12.0 ± 1.8 keV (PDG)	Table 4
$\Gamma(\Upsilon'' \rightarrow \Upsilon\pi\pi)$	1.0 keV	1.72 ± 0.35 keV (PDG)	Table 4
$\Gamma(\Upsilon'' \rightarrow \Upsilon'\pi\pi)$	0.3 keV	1.26 ± 0.40 keV (PDG)	Table 4
$\Gamma(\Upsilon' \rightarrow \Upsilon\eta)$	0.022 keV	< 0.086 keV (PDG)	Eqs.(29) and (30)
$\Gamma(\Upsilon'' \rightarrow \Upsilon\eta)$	0.011 keV	< 0.058 keV (PDG)	Eqs.(29) and (30)
$R' \equiv f_{2010}^{111}(b\bar{b})/m_b ^2 (b\bar{b}) ^3 f_{2010}^{111}(c\bar{c})/m_c ^2 (c\bar{c}) ^3$	0.0025	< 0.0098 (BES, PDG)	Eqs.(32) and (31)
$R'' \equiv f_{3010}^{111}(b\bar{b})/m_b ^2 (b\bar{b}) ^3 f_{2010}^{111}(c\bar{c})/m_c ^2 (c\bar{c}) ^3$	0.0013	< 0.0065 (BES, PDG)	Eqs.(32) and (31)
$\Gamma(\chi_b(2^3P_0) \rightarrow \chi_b(1^3P_0)\pi\pi)$	0.4 keV	–	Table 2
$\Gamma(\chi_b(2^3P_0) \rightarrow \chi_b(1^3P_2)\pi\pi)$	0.002–0.02 keV	–	Table 2
$\Gamma(\chi_b(2^3P_1) \rightarrow \chi_b(1^3P_1)\pi\pi)$	0.4 keV	–	Table 2
$\Gamma(\chi_b(2^3P_1) \rightarrow \chi_b(1^3P_2)\pi\pi)$	0.001–0.01 keV	–	Table 2
$\Gamma(\chi_b(2^3P_2) \rightarrow \chi_b(1^3P_2)\pi\pi)$	0.4 keV	–	Table 2
$\Gamma(\psi(3770) \rightarrow J/\psi\pi^+\pi^-)$	(32–147) keV	$(80 \pm 32 \pm 21)$ keV (BES) (50.5 ± 16.9) keV (CLEO-c)	Table 3, Eq. (45) Eq. (48)
$B(\psi' \rightarrow h_c\gamma)B(h_c \rightarrow \eta_c\gamma)$	$(1.9\text{--}5.8)\times 10^4$	$(4 \pm 0.8 \pm 0.7) \times 10^{-4}$ (CLEO-c)	Eqs. (59) and (60)
$R_\eta \equiv \Gamma(J\psi \rightarrow \gamma\eta)/\Gamma(\psi' \rightarrow J/\psi\eta)$	0.012	0.009 ± 0.003	Eqs. (89) and (90)
$R_{\eta'} \equiv \Gamma(J\psi \rightarrow \gamma\eta')/\Gamma(\psi' \rightarrow J/\psi\eta)$	0.044	0.044 ± 0.010	Eqs. (92) and (94)

6 Summary and outlook

In this paper, we have reviewed the theory and applications of QCDME. We see from Section 3, Section 4 and Section 5 that nonrelativistic QCDME theory gives many successful predictions for hadronic transition and some radiative decay rates in heavy quarkonium systems. Even the simple nonrelativistic single-channel theory can work well for many processes. Although the single-channel approach gives too small rates for $\Upsilon' \rightarrow \Upsilon\pi\pi$, $\Upsilon'' \rightarrow \Upsilon\pi\pi$, and $\Upsilon'' \rightarrow \Upsilon'\pi\pi$ (cf. Table 1), nonrelativistic coupled-channel theory improves the prediction (cf. Table 4). We summarize the above-mentioned main successful predictions for the transition and decay rates in Table 5 together with the corresponding experimental results for comparison.

In addition, the prediction for the $M_{\pi\pi}$ distribution in $\Upsilon' \rightarrow \Upsilon\pi\pi$ from the nonrelativistic coupled-channel theory is in good agreement with the data (Fig. 5).

However, despite the above success, there are experimental results that this simple nonrelativistic approach cannot explain. The CLEO experiment shows a clear double-peak shape for the $M_{\pi\pi}$ distribution in $\Upsilon'' \rightarrow \Upsilon\pi\pi$ [Fig. 6(a)]. Nonrelativistic coupled-channel correction is so small that it cannot account for this shape. Whether this double-peak shape can be explained by the final-state $\pi\pi$ interactions or it is caused by other physical effects is still not clear yet. Further investigation is needed.

Another problem is that in the nonrelativistic single-channel approach, the S -wave to S -wave transitions rates are contributed only by the C_1 term in Eq. (19) due to the orbital angular momentum selection rule, i.e., the obtained $\pi\pi$ angular correlation is isotropic in the laboratory frame. However, experiments on $\psi' \rightarrow J/\psi\pi\pi$ [56] show a small

angular dependence (a 0.2% ingredient of D -wave) of the $\pi\pi$ angular correlation that cannot be explained by the nonrelativistic single-channel theory.⁵ Theoretically, the angular dependence of the transition rates may come from: (a) coupled-channel corrections [state-mixing leads to the C_2 term (D -wave) contributions] and (b) relativistic corrections (orbital angular momentum no longer conserves in the relativistic theory). Actually, the sizes of the corrections (a) and (b) are of the same order of magnitude, and there is interference between them. Therefore to obtain a theoretical prediction for the $\pi\pi$ angular correlation, both (a) and (b) corrections should be taken into account. This means that a systematic relativistic coupled-channel theory of hadronic transitions is expected. So far, there is still no such theory due to the difficulty of dealing with the two-body bound-state equation in relativistic quantum mechanics. There have been various attempts to solve the relativistic

⁵Ref. [56] intended to use a theoretical formula given in Ref. [4] to explain their data on the $\pi\pi$ angular correlation by making a direct comparison of that formula (given in the $\pi\pi$ rest frame in which ψ' is moving) with their partial wave analysis result from their data (done in the laboratory frame in which ψ' is at rest). However, such a comparison is actually inadequate. Since orbital angular momentum is not a Lorentz invariant quantity, partial wave decomposition of a transition amplitude is Lorentz frame dependent. Therefore it is not correct to directly compare the two partial wave decompositions obtained in different Lorentz frames. The correct way of doing it is to make a Lorentz transformation boosting that theoretical formula into the ψ' rest frame, and then make the comparison. It is easy to see that, after the Lorentz boost, the D -wave ingredient in the formula given in Ref. [4] vanishes in the ψ' rest frame, i.e., the theoretical amplitude given in Ref. [4] also leads to an isotropic $\pi\pi$ angular correlation in the ψ' rest frame just as what Eq. (19) does (with $C_2 = 0$). Thus an isotropic $\pi\pi$ angular correlation in the ψ' rest frame is a general consequence of all kinds of nonrelativistic single-channel approaches.

two-body problem. Effort should be made to develop a systematic relativistic coupled-channel theory of hadronic transition.

In summary, the nonrelativistic theory of QCDME approach is not the end of the story. Further development is needed.

Acknowledgment This work was supported by National Natural Science Foundation of China (No. 90403017).

References

1. Gottfried K., In: Gutbrod F. (ed.), Proc. 1977 International Symposium on Lepton and Photon Interactions at High Energies, Hamburg: DESY, 1977, 667; Phys. Rev. Lett., 1978 (40): 598
2. Bhanot G., Fischler W. and Rudas S., Nucl. Phys. B, 1979, 155: 208
3. Peskin M.-E., Nucl. Phys. B, 1979, 156: 365; Bhanot G. and Peskin M.-E., Nucl. Phys. B, 1979, 156: 391
4. Voloshin M.-B., Nucl. Phys. B, 1979, 154: 365; Voloshin M.-B. and Zakharov V.-I., Phys. Rev. Lett., 1980, 45: 688; Novikov V. A. and Shifman M.-A., Z. Phys. C, 1981, 8: 43
5. Yan T.-M., Phys. Rev. D, 1980, 22: 1652
6. Kuang Y.-P., Yi Y.-P. and Fu B., Phys. Rev. D, 1990, 42: 2300
7. Kuang Y.-P. and Yan T.-M., Phys. Rev. D, 1981, 24: 2874
8. Tye S.-H.-H., Phys. Rev. D, 1976, 13: 3416; Giles R. C. and Tye S.-H.-H., Phys. Rev. Lett., 1976, 37: 1175; Phys. Rev. D, 1977, 16: 1079; Buchmüller W. and Tye S.-H. H., Phys. Rev. Lett., 1980, 44: 850
9. Liu D.-S. and Kuang Y.-P., Z. Phys. C, 1987, 37: 119; Bi P.-Z. and Shi Y.-M., Mod. Phys. Lett. A, 1992, 7: 3161
10. Brown L.-S. and Cahn R.-N., Phys. Rev. Lett., 1975, 35: 1
11. Eidelman S. et al. (Particle Data Group), Review of particle physics, Phys. Lett. B, 2004, 592: 1
12. Eichten E., Gottfried K., Kinoshita T., Lane K.-D. and Yan T.-M., Phys. Rev. D, 1978, 17: 3090; Phys. Rev. D, 1980, 21: 203
13. Buchmüller W., Grunberg G. and Tye S.-H. H., Phys. Rev. Lett., 1980, 45: 103; Buchmüller W. and Tye S.-H. H., Phys. Rev. D, 1981, 24: 132
14. Kuang Y.-P., Tuan S. F. and Yan T.-M., Phys. Rev. D, 1998, 37: 1210
15. Bai J.-Z. et al. (BES Collaboration), Phys. Rev. D, 2004, 70: 012006
16. Skwarnicki T., Talk presented at the 40th Rencontres De Moriond on QCD and High Energy Hadronic Interactions, 12–19 March 2005, La Thuile, Aosta Valley, Italy, hep-ex/0505050
17. Partridge R. A., Ph.D. thesis, Report No. CALT-68-1150, California Institute of Technology 1984
18. Schindler R. H., Ph.D. thesis, Report No. SLAC-219, UC-34d (T/E), Stanford Linear Accelerator Center, 1979
19. Adler J. et al., Phys. Rev. Lett., 1988, 60: 89
20. Billoire A., Lacaze R., Morel A. and Navelet H., Nucl. Phys. B, 1979, 155: 493
21. Moxhay P., Phys. Rev. D, 1988, 37: 2557; Ko P., Phys. Rev. D, 1993, 47: 208
22. Kuang Y.-P. and Yan T.-M., Phys. Rev. D, 1990, 41: 155
23. Kuang Y.-P., Phys. Rev. D, 2002, 65: 094024
24. Godfrey S., Z. Phys. C, 1986, 31: 77
25. Heikkilä K., Ono S. and Törnqvist N.-A., Phys. Rev. D, 1984, 29: 110; Phys. Rev. E, 1984, 29: 2136; Ono S. and Törnqvist N.-A., Z. Phys. C, 1984, 23: 59; Törnqvist N. A., Phys. Rev. Lett., 1984, 53: 878; Acta Phys. Pol. B, 1985, 16: 503
26. Chen Y.-Q. and Kuang Y.-P., Phys. Rev. D, 1992, 46: 1165; Phys. Rev. E, 1993, 47: 350
27. Bai J.-Z. et al. (BES Collaboration), Phys. Lett. B, 2005, 605: 63
28. Adam N.-E. et al. (CLEO Collaboration), hep-ex/0508023
29. Bonvicini G. et al. (CLEO collaboration), Phys. Rev. D, 2004, 70: 032001
30. Armstrong T.-A. et al., Phys. Rev. Lett., 1992, 69: 2337
31. Patrignani C., Nucl. Phys. Proc. Suppl., 2005, 142: 98
32. Crystal Ball Group, Annu. Rev. Nucl. Part. Sci., 1983, 33: 143
33. Gross D. J., Treiman S. B. and Wilczek F., Phys. Rev. D, 1979, 19: 2188
34. Rubin P. et al. (CLEO Collaboration), hep-ex/0508037
35. Zambetakis V.-E., Ph.D. thesis, University of California, Report No. UCLA/86/TEP/2
36. Le Yaouanc A., Oliver L., Pene O. and Raynal J.-C., Phys. Rev. D, 1973, 8: 2223
37. Chaichian M. and Kögerler R., Ann. Phys. (N.Y.), 1980, 124: 61
38. Zhou H.-Y. and Kuang Y.-P., Phys. Rev. D, 1991, 44: 756
39. Albrecht H. et al., Z. Phys. C, 1987, 35: 283
40. Green J. et al. (CLEO Collaboration), Phys. Rev. Lett., 1982, 49: 617; Bowcock T. et al. (CLEO Collaboration), Phys. Rev. Lett., 1987, 58: 307
41. Butler F. et al. (CLEO Collaboration), Phys. Rev. D, 1994, 49: 40; Bebek C. et al. (CLEO Collaboration), Phys. Rev. D, 1991, 43: 1448
42. Voloshin M.-B., Pis'ma Zh. Eksp. Teor. Fiz., 1983, 37: 58; JETP Lett., 1983, 37: 69
43. G. Bélanger, DeGrand T. and Moxhay P., Phys. Rev. D, 1989, 39: 257
44. Anisovich V.-V., Bugg D.-V., Saratsev A.-V. and Zou B.-S., Phys. Rev. D, 1995, 51: R4619
45. Lipkin H.-J. and Tuan S.-F., Phys. Lett., 1988, B 206: 349; Moxhay P., Phys. Rev. D, 1989, 39: 3497
46. Komada T., Ishida M. and Ishida S., Phys. Lett. B, 2001, 508: 31; Ishida M., Ishida S., Komada T. and Matsumoto S.-I., Phys. Lett. B, 2001, 518: 47
47. Uehara M., Prog. Theor. Phys., 2003, 109: 265
48. Köner J.-G., Kühn J.-H., Krammer M. and Schneider H., Nucl. Phys. B, 1983, 229: 115
49. Ma J.-P., Phys. Rev., 2002, D 65: 097506; Nucl. Phys. B, 2001, 605: 625
50. Brodsky S.-J., DeGrand T.-A., Horgan R.-R. and Coyne D.-G., Phys. Lett., 1978, 73B: 203
51. Schamberger R.-D. et al. (CUSB Collaboration), Phys. Lett. B, 1984, 138: 225; Csorna S. E. et al. (CLEO Collaboration), Phys. Rev. Lett., 1986, 56: 1222; Albrecht H. et al. (ARGUS Collaboration), Phys. Lett. B, 1987, 199: 291
52. Photiadis D.-M., Phys. Lett. B, 1985, 164: 160
53. Field R.-D., Phys. Lett., 1983, 133B: 248
54. Scharre D.-L. et al., Phys. Rev. D, 1981, 23: 43. See also Königsmann K., Phys. Rep. C, 1986, 139: 243; Köpke K. and Wermes N., Phys. Rep. C, 1989, 174: 67
55. Chang C.-H., Chen G.-P., Kuang Y.-P. and Yi Y.-P., Phys. Rev. D, 1990, 42: 2309
56. Bai J.-Z. et al. (BES Collaboration), Phys. Rev. D, 2000, 62: 032002
57. Fritzsche H. and Jackson J.-D., Phys. Lett. B, 1977, 66: 265